Integration of sedimentology and GPR for high-resolution imaging of a carbonate platform

Stéphan Jorry, Grégory Bièvre

High-resolution imaging of carbonate platform: an integrated approach

STEPHAN J. JORRY[1*] and GREGORY BIEVRE[2,3]

[1] IFREMER, Géosciences Marines, BP 70, 29280 Plouzané Cedex, France

[2] Centre d'Études Techniques de l'Équipement de Lyon, Laboratoire Régional d'Autun, BP 141, 71404 Autun cedex, France.

[3] Laboratoire de Géophysique Interne et de Tectonophysique, UMR-CNRS 5559, Université Joseph Fourier, BP53 38041 Grenoble cedex 9, France.

* corresponding author : stephan.jorry@ifremer.fr

ABSTRACT

Ground-Penetrating Radar (GPR) is a classical technique used for geophysical prospecting of Quaternary shallow subsurface series. Nevertheless, this does not seem to have been widely applied to the recognition of geometries of ancient carbonate platforms. The work presented here reports the results of a sedimentological study combined with GPR prospecting, performed on an Upper Jurassic outcrop located in the southeast Paris basin. A preliminary sedimentological study points out the presence of coral reef bioherms that laterally change into prograding and channeling pure carbonate depositional sequences. GPR profiling, carried out on the top of the cliff, shows an impressive 340 ns two-way travel time (twt) useful range for a 200 MHz antenna, corresponding to a 20-m-depth penetration. The successive GPR profiles illustrate the different bedding planes and major erosional unconformities visible at outcrop, and distinct GPR facies can be individualized. A GPR profile conducted at the base of the cliff has evidenced a strong and continuous reflection level interpreted as a palaeotopographic surface, upon which settled the outcropping biohermal units. These new findings clearly demonstrate the GPR ability for the identification and the interpretation of ancient carbonate platform geometries, ranging between outcrop detailed sedimentological workscale (some few meters) and seismic scale (several hundreds of meters).

Keywords: Paris Basin, Upper Jurassic, Ground-penetrating radar, Coral reefs, Carbonate platform.

INTRODUCTION

Ground-Penetrating Radar (GPR) is a non-invasive, environmentally safe technique for detecting, locating and/or mapping shallow subsurface features. The method uses MHz to GHz frequency pulses to locate natural and/or man-made features of interest. The application of GPR for detecting shallow subsurface heterogeneities has been widely spread during the past few years. Its rapid and easy setting in the field leads to improve studies concerning sedimentary strata, mostly to determine the depth of unconsolidated sedimentary units (i.e. bedrock, permafrost) and to detect buried objects. Conversely, remarkably few studies have examined facies and geometries of carbonate facies. Most such work to date has been dedicated to the characterization of a Middle Silurian bioclastic grainstone megashoal (Pratt and Miall, 1993), to the recognition of facies in Upper Jurassic limestones (Asprion and Aigner, 1999, 2000; Dagallier et al., 2000), and to the characterization of decimeter- to meter-scale sedimentary structures in a Pleistocene oolite shoal-barrier bar setting (Grasmueck and Weger, 2002; Grasmueck et al., 2004). To our knowledge, only one study published by Asprion et al. (2009) focuses on the integration of sedimentology and geophysics to characterize facies and geometries of a carbonate platform in order to interpret facies and geometries on subsurface, when no exposures are available.

The penetration depth of GPR signals in carbonate sequences has been evaluated rather sporadically (e.g. Collins et al., 1994; Sigurdsson and Overgaard, 1998). At a typical GPR frequency of 100 MHz, the expected maximum depth of investigation in such environments is about 10 to 20m. Interestingly, some exposures in the Calcaire de Tonnerre Formation (Upper Oxfordian, Paris Basin) have provided favorable conditions for a GPR survey, allowing a penetration depth of 20m. Based on sedimentological observations conducted during this study, the Calcaire de Tonnerre Formation is represented by carbonate rocks with high facies diversity including coral buildups, adjacent coarse-grain bioclastic flanked deposits, and deep erosive channel-like geometries filled with mudstones. The deposition of these Upper Jurassic facies in the Tethys domain typically reflects the high-carbonate production occurring at the end of the Jurassic, when continental shelves were flooded during an important sea-level rise (Leinfelder, 2001).

This work presents an example of application of GPR to image carbonate platforms. This study combines outcrop information from the Calcaire de Tonnerre Formation with two-dimensional GPR surveys. Main objectives of this study are 1- to define the shape and the

size of the sedimentary packages and their stacking patterns, 2- to map the carbonate sedimentary bodies (coral reefs, prograding clinoforms, large- and medium-scale channel-like features) and large-scale unconformities (erosional surfaces/sequence boundaries) at outcrop and on GPR profiles, 3- to define radar facies according to their sedimentological description at outcrop, and 4- to interpret facies and geometries on an additional GPR survey realized on subsurface, where no exposure is available.

GEOLOGICAL AND GEOPHYSICAL BACKGROUND

Jurassic reefs in the Paris Basin

During the Jurassic, most reefs occurred in the Tethyan realm. Reefs were very rare during the Lower Jurassic (high influx of terrigeneous sediments prevented reef growth in most areas), but the important rise of sea level during the Middle Jurassic has triggered the development of reefs on the northern Tethys shelf which turned into a carbonate-dominated province. Only the Upper Jurassic times provided shelf areas flooded widely enough to provide suitable carbonate ramp settings (Leinfelder, 2001). A large part of the European continent was covered with shallow epireic seas connected to different sedimentary basins (Paris, Dauphinois and Aquitaine deep marine environments) and marginal to the Tethys Sea to the south (Fig. 1). In Western Europe, the shallow marine carbonate production was preferentially distributed around the Massif Central between 20° and 30° of latitude.

General comparative studies of Late Jurassic reefs in western Europe have recognized a number of distinct reef types – coral, sponge, microbial – based on their taxonomic composition and their paleoecological and sedimentological characteristics (Beauvais, 1973; Crevello and Harris, 1982; Gaillard, 1983; Leinfelder, 1993; Werner *et al.*, 1994; Leinfelder *et al.*, 1994; Insalaco, 1996; Schmid, 1996; Insalaco *et al.*, 1997; Helm and Schülke, 1998; Dupraz, 1999; Dupraz and Strasser, 2002; Olivier *et al.*, 2004). The Upper Oxfordian reefs from the southern margin of the Paris Basin are strictly dominated by corals. About 130 genera in the Upper Jurassic are described, in a time interval coinciding with sea level rise, shelf expansion and warm climatic conditions with periods of high sedimentation rates (Leinfelder *et al.*, 1994; Bertling and Insalaco, 1998). An important climatic change appears to have occurred during the Middle to Upper Oxfordian transition, initiating major reefal development in the Swiss Jura and in other regions of the northern shelf margin of the

Tethys (Gygi, 1986; Gygi and Persoz, 1986; Pittet, 1996; Pittet and Strasser, 1998; Pittet *et al.*, 2000; Cecca *et al.*, 2001; Olivier *et al.*, 2003, 2004). At the beginning of the Upper Oxfordian, abundant rainfall caused terrigeneous sediment input and resulted in a more mixed siliciclastic/carbonate system (Olivier *et al.*, 2004).

The study area is located in the SE of the Paris Basin (Fig. 2) and focuses on the Calcaire de Tonnerre Formation. Several studies describe Upper Oxfordian reefs on the southern margin of the Paris Basin (Menot and Rat, 1967; Menot, 1974, 1980; Insalaco, 1996; Chevalier *et al.*, 2001), known as the Chatel Censoir biostromes. Chronostratigraphically, they occur between the top of the *Transversarium* Zone and the top of the *Bifurcatus* Zone (Fig. 2). The Upper Oxfordian deposits from the Calcaire de Tonnerre Formation have received very little scientific attention. Sedimentological and stratigraphical studies of the Calcaire de Tonnerre Formation were carried out by Lambert (1893), Loreau (1967) and Loreau and Tintant (1968). Following an ammonite revision (Hantzpergue, oral communication), this Formation spans the Planula zone (Fig. 2). The dominant facies is a pure micritic and chalky limestone (99.5% of $CaCO_3$), whereas subordinate amounts of pelletal and oolitic packstones also occur. Pure oolitic facies are known as «Pierre de Tonnerre» (Loreau, 1967) but these facies are absent from the entire studied outcropping succession.

Several small coral bioherms and coral-rich debris breccia facies have been described from the Formation (Loreau and Tintant, 1968), but plurimeter-scale coral edifices were documented during this study. The growth of coral reefs in the Calcaire de Tonnerre, partly composed of microsolenids, led to the development of significant syndepositional reliefs which occurred during the Planula biozone. This period has produced reefs that grew under moderate to high-energy settings, in a pure carbonate environment.

Application of GPR in carbonate facies

The potential of GPR as a tool for mapping and detecting shallow subsurface heterogeneities in different geological settings has been clearly demonstrated during the past few years. In limestone series, it is assumed that changes in electrical properties are mostly related to petrological or structural changes (Pratt and Miall, 1993; Meschede et al., 1997; Asprion and Aigner, 2000). Recent works have also demonstrated the potential of GPR for investigating limestone cliffs in terms of fracture assessment (Jeannin et al., 2006; Deparis et

al., 2007).

However, few successful attempts to determine the bedding geometries in carbonate series have been referenced. Pratt and Miall (1993) briefly document the internal architecture of a reservoir-scale grainstone shoal deposited during the Middle Silurian by using a GPR. They demonstrated the first instructive example for using GPR on carbonate strata (composed of almost pure dolostone) which are lithologically homogeneous. Asprion (1998) and Asprion and Aigner (2000) demonstrated the possibility of using this tool for carbonate facies recognition in Upper Jurassic limestones, especially reef buildups which form hydrocarbon reservoirs (e.g. Crevello and Harris, 1982; Sun and Wright, 1998). Dagallier et al. (2000) also carried out a GPR survey in Upper Jurassic limestones. Their work outlined several depositional units (high-energy grainstones and low-energy mudstone) and different carbonate lithologies recognized with distinct GPR reflections. Grasmueck et al. (2004) used GPR to image in 3D decimeter- to meter-scale sedimentary structures in a Pleistocene oolite shoal-barrier bar setting, and demonstrated that GPR signals can be transformed into clear images of a complex shallow-subsurface anatomy.

Recently, Asprion et al. (2009) proposed a new approach consisting in using GPR sections for extrapolating facies information and geometries from outcrops and wells in order to refine and extend the resolution of the medium- and small-scale complexities in facies architecture on the Tortonian carbonate ramp of Menorca. This approach, known as outcrop analogue approach, is classically used in petroleum geology in order to characterize subsurface reservoirs (e.g. Hornung and Aigner, 2002; Jorry et al., 2003; Pringle et al., 2004). In subsurface geophysics applied to sedimentary strata, it has been mainly developed for 2D and 3D characterization of clastic reservoirs (McMechan et al., 1997), glaciofluvial deposits (Beres and Haeni, 1991, Beres et al., 1995, 1999) with applications to aquifer reservoir modelization (Asprion and Aigner, 1999; Heinz and Aigner, 2003; Huggenberger and Regli, 2006) and to hydrostratigraphical characterization (Goutaland et al., 2008). To our knowledge, Apsrion et al. (2009) are proposing the first study focusing on the integration of sedimentology and geophysics to characterize facies and geometries of a carbonate platform, although they provide well-defined geometries with unmigrated GPR data. The important penetration depth gained by Asprion et al. (2009), representing almost 400 ns with a 300 MHz antenna, clearly illustrates the contradiction between the recent (last decade) high spreading in using GPR and the very few attempts to characterize carbonate environments with a proved powerful technique.

MATERIALS AND METHODS

Sedimentological and petrophysical studies

This study focuses on an outcrop located close to the city of Tonnerre, in the Armançon valley in France. Upper Oxfordian and Lower Kimmeridgian carbonate rocks are exposed along a recent roadcut (Fig. 2 and Fig. 3).

The geometry of stratal terminations in the field allows the recognition of several unconformities and the establishment of the architecture of plurimetric sedimentary packages and sequences. Erosional surfaces separate coral reefs, dunal offlap beds, and intercalated thin subhorizontal beds. Facies from each sedimentary package (reef and inter-reef zones) have been described in the field and sampled. Petrographic analysis (textures, faunal content and diagenetic features) provided critical information for interpreting both depositional environments and unconformity surfaces. Moreover, relative paleobathymetrical estimations are based on the morphology of corals (lamellar, branching and massive forms), the associated microfauna (algae, foraminifers) and macrofauna (sponges, serpulids, oysters, gastropods, brachiopods), and the nature of the matrix of the reefs (carbonate mud, bioclastic sands).

Examination of stratigraphic sequences and the age-interpretation of unconformity surfaces provide evidence for the interpretation of major sedimentary events (i.e. deposition and erosion periods). Depositional sequences are defined as a relatively conformable succession of genetically related strata bounded by unconformities or their correlative conformities, whose base and top are limited by sequence boundaries that result from erosion during fall of relative sea level. The stratigraphic succession of these boundaries can be used to follow the architectural evolution of the carbonate platform.

Samples were cored at outcrop using a field corer. Plugs, which average size is about 3 cm length and 2.5 cm of diameter, have been dried at 50°C during two days. Permeability measurements were made using a PMI GP-262 Gas Permeameter housing at Geneva University. The principle consists in measuring the air quantity which goes through the sample. A rubber shaft is placed around the plug to provide a good waterproofness. The gain is fixed around the plug in a pressurization chamber (7 bar). The pressure is progressively increased at the base of the sample, and the outgoing pressure is measured at the other

plug extremity. The permeability is defined by Darcy's Law:

$$Q = \frac{(P_1 - P_2).S.k}{\mu.L} \quad (1)$$

With:
Q= units of volume (cm^3/s),
P1, P2= enter and exit pressure, respectively (atm),
S= sample section (cm^2),
K= permeability (Darcy),
M= absolute fluid viscosity (centipoises),
L= sample length (cm).

Bulk rocks were used to determine carbonate content. Carbonate contents were analyzed using a carbonate bomb (Müller and Gastner, 1971; Droxler et al., 1988). About 2 cm^3 of sample were placed into a sealed vessel and reacted with 10% HCl (2.3 mol/l). The volume of CO_2 released was compared to volumes released by reacting known amounts of 100 % of $CaCO_3$.

Ground-penetrating radar principles

The GPR technique is used to obtain a high resolution image of the subsurface. An electromagnetic (EM) pulse is sent into the ground via a transmitter at a determined central frequency. Frequencies classically range between 50 Mhz and 1 Ghz (radio waves). This pulse propagates through the ground and, at each interface between two different materials (in terms of electromagnetic difference), a part of its energy is reflected towards the surface. The successive echoes are recorded according to the time range by the receiver (Daniels, 1996). GPR prospecting is then an EM analogue technique to reflection seismic. The EM wave energy is progressively attenuated in depth by the materials. The penetration depth depends on several factors, the most important being the dielectric constant (or relative permittivity) of the surrounding medium which is closely related to its electrical conductivity. The dielectric constant is linked to the petrology and structure of the materials (e.g., clay content, porosity) as well as water content, especially at the ground near surface. In first

approach, in resistive medium, the wave propagation velocity *v* can be represented in the following form:

$$v = \frac{c}{\sqrt{\varepsilon_r}} \quad (2)$$

With:

v = EM wave velocity (m/s),

c = EM wave velocity in the void (= $3x10^8$ m/s),

ε_r = relative permittivity (without dimension).

The wave energy attenuation α can be simplified as shown in equation 3. It shows that the relative permittivity is the main factor controlling the attenuation: the lower is the relative permittivity (and hence, for earth materials, the electrical conductivity), the greater is the attenuation.

$$\alpha = \frac{1}{2c\varepsilon_0} * \frac{1}{\rho\varepsilon_r} \quad (3)$$

With:

ε_0 = void electric permittivity (without dimension).

ρ= resistivity of the material at the considered frequency (ohm.m),

As usual in geophysics, there is a trade-off (and hence a choice to be made) between penetration depth and resolution, which is linked to the emitted wave length. A long wavelength causes a low attenuation and the EM wave will penetrate deeply. Correlatively, the resolution is low and the wave is not affected by small objects. Vertical and horizontal resolutions are estimated for a single antenna/reflector way path, according to the wavelength (λ). Vertical resolution is theoretically equal to the quarter of the wavelength of the central return frequency (i.e. frequency for which maximum energy is backscattered). It can be defined as follows:

$$r_v = \frac{\lambda}{4} = \frac{c}{4f_c\sqrt{\varepsilon_r}} \quad (4)$$

With:

r_v = vertical resolution (m),

λ = EM wavelength (m),

f_c = central return frequency (Hz).

In practice, nevertheless, the vertical resolution is often estimated between the third and the half the wavelength (Beres and Haeni, 1991). The horizontal resolution corresponds to the Fresnel zone diameter, which is the circular zone centered on the reflexion point contributing, the most to the reflexion. It can be calculated using equation 5 (Daniels, 1996):

$$r_h = \sqrt{\lambda \frac{^2}{16} + \frac{zh}{2}} \quad (5)$$

With:

r_h = horizontal resolution (m),

z = depth of the reflector (m).

GPR processing and interpretation

GPR measurements were performed using a SIR 3000 system developed by GSSI (Geophysical Survey System Inc.), associated with 200 MHz and 400 MHz shielded antennas operating in monostatic mode (a single antenna is used to transmit and to receive the electromagnetic pulses). In addition, the topography was calibrated with differential global positioning system (D-GPS) measurements realized every 10 m along the profiles.

The GPR surveys were concentrated on outcrop DEV1 only, the accessibility on top of outcrop DEV2 being not appropriated for an optimal GPR acquisition. Profiles conducted on the top of the hill were far enough from the cliff to prevent side-effect, but however close enough to allow a direct analogy between GPR images and outcrops. The different acquisition tracks were clean and rather tabular, allowing recordings in a continuous mode. The GPR was dragged along the ground at a slow and rather constant walking speed. A 40 scans/s rate was selected in order to a posteriori enhance the signal/noise ratio with a stack operation when normalizing the GPR profiles in distance.

GPR processing sequence is summarized in Table 1. The data were processed using the Reflexw package (Sandmeier Scientific Software; Sandmeier, 2007). Several filtering and

gain adjustment operations were performed to enhance the data quality. Time-zero correction was used to align the whole traces to a same origin in time. Dewow and background removal removed low frequency system-dependent noise and high amplitude permanent temporal noise, respectively. Profiles were bandpass-frequency filtered, centered on 120 Mhz (corresponding to the nominal return frequency of the 200 MHz profiles). The bandpass frequencies are given in Table 1. To compensate for the EM energy attenuation with time, an energy decay gain correction was applied to the signals.

To reflect the true geometry of heterogeneities and interfaces in respect with depth, topography correction and migration operations were employed. Migration is a mathematical operation which consists of precisely re-locate reflectors in depth (or in time), i.e. to track back the energy of the reflection to its source. Two main migration techniques, both with constant velocity, have been tested during this study. The Kirchhoff migration, conducted in the distance/time range, is based on a summation along hyperbola curves. The frequency/wave number migration conducted in the spectral mode was preferentially applied for this study. This second migration technique is more appropriated to the migration of extended or steep reflectors (Sandmeier, 2007).

The outcrop calibration of GPR images on remarkable reflectors at different depths gives a 0.12 m/ns EM wave velocity, which is typical within these media (e.g. Reppert et al., 2000; Neal, 2004). The time range used in this survey provides good quality data up to 340 ns two-way travel time (TWT) with the 200 MHz central frequency antenna for the P1 profile. Based on this calibration, up to 20 m depth of penetration was reached by using the 200 MHz antenna.

The GPR profiles were interpreted with the Kingdom Suite package (Seismic Micro-Technology, Inc.), in terms of radar facies and radar surfaces, according to Neal (2004). The interpretation of the GPR images consists of identifying and picking lateral terminations such as downlap, onlap and toplap. Based on the outcrop calibration, radar facies can be interpreted in terms of sedimentary facies and sedimentary units.

RESULTS

Sedimentological description

This section is dedicated to the description and interpretation of the main

sedimentary bodies and of successive depositional sequences. The large-scale observation of the outcrops located along the roadcut of Tonnerre shows the superposition of several accretional units separated by erosional surfaces (Fig. 4). These units are composed of decimeter to meter-scale carbonate beds prograding toward the SW. In closer observations, a more detailed sedimentary pattern revealed the presence of several coral-dominated buildups with steep flanks, which are intercalated in different accretional units.

Coral buildups are variable in size (Fig. 4). The biggest bioconstruction on the outcrop DEV1 is a 20-m-wide and 20-m-high reef complex with a high biotic diversity. An unconformity surface (DT1) divides this unit in two amalgamated reefs (R1 and R3). The R1 reef, exclusively composed of dish corals, shows a mudstone matrix. Branching and massive corals dominate the R3 reef and are associated with peletoidal packstones and grainstones. Facies on both flanks of these reefs change rapidly into stratified coarse bioclastic rudstones dominated by peloids and bioclasts. Smaller bioherms are also visible at the base of the outcrop DEV1. The R2 reef shows a coral assemblage similar to that of the R1 reef. The R4 bioherm is characterized by abundant thick and large dish corals, and internal sediment is composed of coarse bioclastic debris (Fig. 4). Facies on the northeastern part of this bioherm grade of lateral prograding flank beds of packstones composed of materials derived from the R4 reef core. The top of the R4 bioherm is an irregular erosion surface that truncates both corals and internal sediment, and it is overlain by packstones (Fig. 4 and Fig. 5-c). This unconformable surface occurred after the lithification of the internal sediment between builder organisms.

Lateral to the coral reefs, unconformities and their correlative conformities can be easily identified (Fig. 4). Lateral to the R1-R3 reef complex, bioclastic rudstone facies prograde toward the south forming clinobeds with an average dip of 15°. The top of this accretional unit is bounded by unconformity DT2 and crosses the R3 reef. Another prograding body, capped by an erosive surface (DT3), corresponds to well-stratified packstones arranged in large sigmoid prograding beds (Fig. 5-a). This prograding interval contains some well-preserved, overturned branching corals, and large blocks composed of a coral-dominated framework, attesting to the erosion of coral mounds and the accumulation of coral rubble (variable in size) along the reef talus. The other accretionary units are mostly dominated by the deposition of subhorizontally stratified wackestone/mudstone facies. The top of these accretionary units, whose bases and tops are bounded by unconformities DT4 and DT5, is characterized by the presence of medium-scale channels eroding the uppermost

horizontal beds of the Calcaire de Tonnerre Formation. These channels are filled with mudstones and exhibits poorly sorted bioclastic facies at their base, made up of peloids, skeletal fragments (500µm to 2cm in size) and coral debris. The erosional surface corresponds to the unconformity DT6.

The outcrop DEV2, located on the other side of the roadcut, allows the documentation of the carbonate system in 3D (Fig. 4). Coral-dominated reefs and off-reef prograding facies can be correlated by well defined sequence boundaries (DT1 to DT5), but the general architecture significantly differs from the DEV1 outcrop. Correlations between both facing outcrops based on the presence of patch reef made of dish corals, that coincides with the DEV1 R1 and R4 reefs (Fig. 4-c: facies f1), and by a good geometrical relation of the DT4 unconformity. The R2 reef does not continue to the DEV2 outcrop.

The complexity of the platform architecture is accentuated by the occurrence of branching coral-dominated reefs (R3, R5 and R6 reefs) above the DT2 and DT4 sequence boundaries (Fig. 4 and Fig. 5-b). Branching corals are similar to the DEV1 R3 reef and are represented by the same species, i.e. *Calamophylliopsis* sp. and *Pseudocoenia* sp. (Fig. 4-c: facies f3). Inter-reef facies are composed of packstones-grainstones that occasionally contain decimetric blocks resulting from the erosion of the reefs (Fig. 4-c: facies f2). At the DEV2 outcrop, some metric blocks occur below the R3 and R6 reef units at DEV2 (Fig. 5-b). The deposition of coral rubble below the R6 reef might be synchronous to those observed at DEV1. The presence of reef debris confirm that high-energy settings prevailed during a depositional sequence delimited by DT2 and DT3 unconformities, leading to a significant erosion of the reefs.

The marked lateral facies changes in the two facing outcrops demonstrate the complexity of the platform facies architecture. The growth of dish coral-dominated reefs is synchronous and laterally homogeneous on the carbonate platform, while branching coral-dominated reefs constitute more isolated structures with a limited lateral extension. In general, the presence of large blocks and grainstone/packstone facies in the inter-reef areas confirm that the patch reefs grew in moderate to high-energy settings. The reefs are capped by the DT5 boundary, which is overlain by mudstones/wackestones (Fig. 4-c: facies f4).

Event stratigraphy: chronology of unconformities and sedimentary fillings

Six depositional sequences have been identified within the Upper Oxfordian Calcaire

de Tonnerre Formation. Each sequence, whose base and top are delineated by sequence boundaries (DT), is characterized by a succession of accretional units. We propose to illustrate the architecture of the carbonate platform from sequence S1 to sequence S5, by establishing the correspondence of stratal geometries, depositional facies, and sequences between the DEV1 and DEV2 outcrops (Fig. 6).

a. Sequence 1 (S1)

i. Facies and Biota: This sequence is characterized by the early settlement of R1 and R2 dish corals (Microsolenidae and *Actinaraea* sp.) in a bathymetric range of 30 to 40 m depth. Associated fauna is dominated by calcisponges (Chaetetidae) and gastropods, with some bioclastic elements encrusted by nubeculariids and algae (*Cayeuxia* sp.). A coarse bioclastic fringing facies accumulated lateral to the incipient reef structures.

ii. Stratal Geometries: The dish corals constructed metric to plurimetric patch reefs. The R1 reef can be subdivided into several accretionary units that are separated by undulated erosional surfaces. Coarse bioclastic debris accumulated as prograding packstones in peripheral beds.

iii. Bounding Surface Description: The base of this sequence is not visible. The unconformity (DT1) at the top of R1 and R2 reef structures is a sequence boundary, which defines the paleotopography of the carbonate platform.

iv. Interpretation: *Lithophaga* borings on the undersides of *Actinaraea* lamellas in the R1 reef are evidence of a well-illuminated paleoenvironment. Lateral accumulation of coarse bioclastic packstones indicates synsedimentary erosion of the reef mounds. At the top of the R1 reef, the DT1sequence boundary attests to a significant fall of the relative sea level.

b. Sequence 2 (S2)

i. Facies and Biota: Growth of the first branching corals in the R3 reef occurred at few meters of water depth. Branches are sparsely encrusted by micrite (trombolites?) and by calcisponges. Lateral facies are prograding packstones/grainstones containing common coral fragments. Coral rubble containing metric blocks of dish coral facies are laterally flank to the R3 reef (visible at outcrop DEV2).

ii. Stratal Geometries: The internal architecture of the R1-R3 reef on DEV1 outcrop is characterized by superimposed aggradational reef packages. The branching coral-

dominated reef changes laterally into stratified grainstone facies.

iii. Bounding Surface Description: The base and top of this sequence are bounded by the unconformities DT1 and DT2. The DT2 boundary truncates clinobeds deposited during the previous sequence S1.

iv. Interpretation: The lateral facies transition into prograding packstones containing common coral fragments indicates synsedimentary erosion of the R1-R3 reef. The reef aggradation indicates a progressive sea-level rise, attesting to a keep-up growth strategy (Kendall and Schlager, 1981).

c. Sequence 3 (S3)

i. Facies and Biota: This sequence is characterized by the deposition of clinobeds containing large fragments of reefal units, mainly represented by branching and massive coral-dominated facies. The top of a large block which is visible at outcrop DEV1 is encrusted with oysters. Growth of a new bioherm (R4) attests to the proliferation of encrusting and unbored dish (*Actinaraea* sp.) and massive corals.

ii. Stratal Geometries: Accretionary units containing large coral fragments form prograding sedimentary clinobeds. The R4 bioherm is a well-cemented reef structure that has a sharp contact with the lateral prograding fringing facies.

iii. Bounding Surface Description: The top of this depositional sequence is the truncating DT3 sequence boundary. Erosion most probably resulted from a displacement of subaqueous dunes or change in the flow pattern.

iv. Interpretation: The accumulation of coral rubble from erosion of the reef mounds attests to continuous high-energy conditions. The encrustation by oysters at the top of some blocks indicates a decreased sedimentary rate. The presence of overturned branching corals in the prograding wedges confirms active erosion of the higher part of the R3 reef. Erosion might represent a significant hydrodynamic event, such as the displacement of dunes or change in current regime.

d. Sequence 4 (S4)

i. Facies and Biota: This sequence is composed of packstones/grainstones, branching and massive-coral reef facies, and the mud-rich carbonates with a diverse fauna including massive corals (*Thamnasteria lomontiana*) growing on *Trichites* shells. Inter and off-reef facies are composed of coarse bioclastic packstones/grainstones containing coral fragments.

ii. Stratal Geometries: Aggrading coral facies contribute to the development of two

plurimetric bioherms (R5 and R6) characterized by steep flanks and separated by fringing clinobeds. The muddy accretionary unit is poorly stratified. The progradation of large clinobeds continue to the southwest.

iii. Bounding Surface Description: The sequence is bounded at its top by the DT4 sequence boundary. Unconformities at this boundary show a considerable erosion of sediment volume. This boundary cut down through sequence the S3 sequence.

iv. Interpretation: This unit represents sedimentation in more quiet areas surrounded by coral mounds, with low sedimentation rate, where carbonate mud precipitation and deposition occurred (Loreau, 1975, 1979, 1982). The initial development of coral colonies suggests a stable substratum of *Trichites* shells that were fixed into the sediment. The geometry of sequence boundaries suggest that the sedimentary package is only a relic of a larger depositional sequence, including dunal and interdunal environments. A capping DT4 sequence boundary records a significant fall of the relative sea level.

e. Sequence 5 (S5)

i. Facies and Biota: This depositional sequence is dominated by the deposition of mudstones/wackestones that are devoid of coral fragments and of other skeletal components. Reefs that grew laterally are dominated by branching (phacelloid *Calamophylliopsis* sp. and ramose *Pseudocoenia* sp.) and massive growth corals.

ii. Stratal Geometries: The muddy deposits onlap and downlap onto the DT4 unconformity. A significant period of reef growth constructed the plurimetric R6 bioherm, which is composed of several reef packages.

iii. Bounding Surface Description: The top of this depositional sequence is bounded by the DT5 sequence boundary, the last sequence boundary visible at outcrops. This boundary pinches on the DT4 unconformity.

iv. Interpretation: The occurrence of a high proportion of carbonate mud in this facies deposited indicates a change in the energy of the depositional environment. In the study area, this change might represent the infilling of large incised channels or may characterize distal parts of large bedforms.

f. Sequence 6 (S6)

i. Facies and Biota: This last exposed depositional sequence is characterized by mudstones/wackestones and poorly sorted bioclastic limestone that is composed of 500µm – 2cm bioclasts and large debris of *Diceras*.

ii. Stratal Geometries: Horizontally bedded mudstones/wackestones onlap the DT5 unconformity and bury all reefs. The top of the platform is eroded by small meter-scale channels.

iii. Bounding Surface Description: The top of this depositional sequence is bounded by the DT6 sequence boundary and is characterized by channels that erode the top of the Upper Oxfordian carbonate platform.

iv. Interpretation: The erosive channels, which cut the upper Calcaire de Tonnerre, indicate a period of low relative sea level. These channels might be induced by wave- or tide-driven currents.

The architecture of the depositional sequences and sequence boundaries outline the depositional scheme of the Upper Oxfordian carbonate platform near Tonnerre. Fig. 6 presents an interpretation of the development of the successive sequences, including processes, resulting morphologies and inferred oscillations of relative sea level. Relative sea level fluctuations produced major changes in carbonate production, expressed by the occurrence of different coral communities. The development of coral reefs was active during time intervals characterized by the highest rises of the relative sea level. Branching coral-dominated reefs preferentially grew after significant drops of the relative sea level, as occurred at sequence boundaries DT1 and DT4. The exclusive occurrence of these keep-up reefs indicates high-energy conditions and a very shallow water depth at the top of the bioherms. The concurrence of branching- and thick-braided platy coral-dominated reefs during the S3 sequence indicates a period of high sedimentation rate. The edification of branching coral reefs prevailed in shallow water settings and in the same time, thick-braided *Actinarea* reefs grew in deeper and turbid conditions at the base of prograding bioclastic clinoforms. Other sequence boundaries, i.e. DT3 and DT5, result from erosion during minor drops of the relative sea level. Between sequence boundaries, other unconformable surfaces are mostly interpreted as the result of erosion initiated by storms or by changes in current regimes.

Calibration of GPR facies with outcrop lithofacies

GPR profile P1 (Fig. 7) conducted at the top of the cliff DEV1, directly correlated with the 25-m-high outcrop, shows an impressive 340 ns TWT useful range for the 200 MHz

antenna corresponding to a 20-m-depth penetration with a velocity of 0.12 m/ns. Furthermore, the raw data clearly show very little noise. In addition with a detailed sedimentological description of the different cropping units, the analysis of this GPR profile allows the recognition of bedding planes and major erosion surfaces (i.e. sequence boundaries), and the individualization of sedimentary facies characterized by distinct GPR surface and facies (Fig. 8).

Coral buildups have visible internal bedding at outcrop. The associated reflection pattern is mostly characterized by numerous strong and discontinuous reflections variable in amplitude (Fig. 9, Loc.1). They might be generated by non-uniform cementation and heterogeneous matrix content of the reefs. Furthermore, zones of flat- and convex-dominated reflection shapes can be distinguished, and appear to correspond to dish- and branching-coral dominated reef facies, respectively (Fig. 9, Loc.1). The presence of a megaboulder (coral rubble), derived from the erosion of coral buildups, has been clearly identified at outcrop DEV1 (Fig. 5). The corresponding radar facies coincides with hyperbolic shaped reflections.

Deposition of prograding bioclastic facies lateral to the coral reefs clearly result from production and exportation of carbonate products derived from growth and erosion of coral reefs. Radar facies, characterized by mostly continuous, sub-tabular to sigmoid/oblique reflectors with various amplitude width and frequencies, illustrate the accumulation of bioclastic facies on the reef flanks and within inter-reef depressions (Fig. 9, Loc. 2). Major erosive unconformities within the flanked prograding facies can be also distinguished on GPR. The basal contact is generally oblique or tangential, while the upper contact is onlapping or toplapping. These major unconformities are characterized by high amplitude reflections and can be easily individualized and classically picked by pointing lateral reflector terminations.

Medium-scale channels were clearly identified on the GPR survey P1 carried out on the top of the outcrop DEV1 (Fig. 3), using a 200 Mhz antenna. Focus on these channels, a 50-m-long survey realized with a 400 Mhz antenna (P2) shows a detailed picture of the internal structure of these channels (Fig. 9; Loc. 4). They appear individualized by an erosive surface at their base, and GPR pattern, characterized by continuous, sub-parallel concave reflections (less and less concave from base to top), clearly onlap the channel flanks. These geometrical features correspond with channel-filled sequences, as defined by Mutti & Normark (1987, 1991), and are exclusively filled with mudstones. Below the channels, this

GPR survey has revealed also the presence of localized, strong and discontinuous, convex shaped, high amplitude reflections, which can be interpreted as coral reefs.

The cap mudstone facies occur at the top of the facies succession and overlay carbonate buildups and their prograding flanked facies. At outcrop, they include well stratified thin-bedded mudstones which contain very few disseminated bioclasts. Prominent moderately continuous reflector lines are interpreted to correspond to the thin-bedded mudstones at the top of the cliff. GPR profiles also show moderately concave to hummocky shapes with onlap terminations on the flanks and some indications of basal truncation as well. Based on geophysical data analysis and sedimentological information, these cap mudstones may be defined as constituting a large-scale erosive channeling sequence at the top of the Upper Oxfordian series (Fig. 9; Loc. 4).

Two main reflection-free zones at the beginning and at the end of P1 have been observed (Fig. 7). These could be attributed to a homogenous massif (no EM constrast). In this case study, the occurrence of reflection-free zones coincides with the presence of a thin top soil layer which strongly attenuates the EM wave energy. This clearly illustrates the strong influence of conductive layers on the GPR response.

Some of the specific radar facies have been sampled at outcrop for running petrophysical analyses. Table 2 summarizes the main petrophysical properties of several facies collected in prograding flanking units, lamellar coral patch-reef, and muddy channeling depositional sequence. The measurements indicate that the whole plugs have a 100% of $CaCO_3$ content (see Fig. 7 for samples location). The absence of any electrically conductive particles such as clay in the Calcaire de Tonnerre Formation may explain the important penetration depth which has been reached in this case study. On the other hand, while porosity of the different sedimentary units is rather similar, a permeability contrast is observed between reefal/peri-reefal units and muddy channeling facies.

Geometries and facies occurrence in subsurface

Once GPR facies are calibrated with outcrop lithofacies, the objective is to get some information regarding depositional geometries and facies below the outcropping unit of the Calcaire de Tonnerre, in particular to image the base of the outcropping coral reefs. The questions are the following: do we have a drastic change in term of depositional facies and environment through the Calcaire de Tonnerre Formation? Does the base of coral reefs

visible at outcrop correspond to the base of the reef edifices? If not, what are the nature and the morphology of the substratum at the base of the bioherms?

In order to answer to these questions, an additional GPR survey (P3) has been conducted at the base of the cliff DEV1 (Fig. 3). This survey shows a penetration depth of 11 m, corresponding to a 190 ns twt range with a velocity of 0.12 m/ns (Fig. 10). Different GPR facies, geometries, and unconformities can be distinguished and are in good continuity with profile P1. Based on the previous outcrop calibration, this survey indicates that the same depositional settings prevailed before the growth of the coral reefs. Radar facies can be interpreted as dominant high-energy bioclastic facies, organized in large-scale prograding sequences which are delimited by erosive unconformities (Fig. 9, Loc.3). Also, several medium- to large-scale channels can be individualized by erosive base and sigmoid beds (Fig. 9, Loc. 6). No major coral reefs are detected on this profile P2.

The superposition of both GPR profiles made at top and base of the outcrop DEV1 gives a 30 to 40-m-thick image of the whole carbonate platform, going from the reefs settlement to their burying (Fig. 11). On profile P3, some reflectors are characterized by strong and continuous reflections, in particular one of them which is visible all along the profile. This major reflector suggests a major erosion on top of bioclastic beds and can be interpreted as a palaeotopographic surface, upon which settled the outcropping coral reefs.

DISCUSSION

Implications for Upper Jurassic reefs

This case study is the first published example dealing with the complete evolution of a coral-dominated reef carbonate platform (from the initiation of submarine highs to the platform infilling) in a pure carbonate environment from the Upper Jurassic. The morphology of the depositional profile from Tonnerre's platform was dominantly controlled by allocyclic processes (variations of relative sea level) which induced major erosional events at sequence boundaries, and reef aggradation during periods of accommodation increase. Autocyclic processes (such as storms or change in current regime) might have contributed to the reefs' erosion, leading to the accumulation of coral rubble along the reef talus.

Moreover, considering that the Calcaire de Tonnerre Formation was deposited during the Planula zone, it appears reasonable to propose a time range for deposition about 500

kyrs, during which five sea-level falls have been recognized. Taking into account that reefs grew on the stable and wide shelf of the northern Tethys margin, it strongly suggests that the high-frequency, moderate to low amplitude eustatic fluctuations that have been detected in the Planula zone were not driven by tectonic pulses. In terms of sequence stratigraphy, Upper Jurassic first and second order sea-level changes were controlled by tectono-eustatism, the major cause probably being the expanse of mid-oceanic ridges during the breakup of Pangea (Leinfelder, 1993, 2001). Causes for third and higher order sea-level fluctuations remain unclear, and a strong controversy exists in the interpretation of the Upper Jurassic climate. The Upper Jurassic is mostly characterized by “greenhouse” type conditions. Most of available $\delta^{18}O$ data suggest the onset of a warming phase throughout the Middle-Upper Oxfordian (Hoffman et al., 1991; Price and Sellwood, 1997; Price and Gröcke, 2002; Wiezbowski, 2002, 2004; Gröcke et al., 2003). Moreover, global biochemical models predict high pCO_2 levels (Berner 1994), and simulations of climatic regimes using General Circulation Models do not rule out the seasonal formation of ice caps (Moore et al., 1992a, 1992b; Ross et al., 1992; Valdes and Sellwood, 1992; Sellwood and Valdes, 1997; Sellwood et al., 2000). However, based on sea surface paleotemperature values calculated on oxygen isotopes of low-Mg calcitic and aragonitic shells from tropical seawater, Veizer et al., (2000) proposed an icehouse mode for the Upper Jurassic. To explain the apparent contradiction with high pCO_2 levels, the authors suggested that atmospheric carbon dioxide concentrations were not the principal driver of climate variability, at least for the Upper Jurassic. This icehouse mode is confirmed by a recent work published by Dromart et al. (2003) evidencing that the Upper Jurassic climate is characterized by ″…brief and global cooling affected sea surface temperatures at the Middle-Upper Jurassic transition (around the Callovian-Oxfordian boundary), and was plausibly associated with the formation of subpolar continental ice″. The authors also indicates that the magnitude of refrigeration was about 1-3°C for lower middle latitudes, and coincides in time with an abrupt global-scale fall of sea level documented through sequence stratigraphy (Haq et al., 1988).

The formation of continental ice is known as the most efficient mechanism to account for rapid, global-scale sea-level change. Taking into account that cooling events occurred at the Upper Jurassic (Veizer et al., 2000; Dromart et al., 2003) and the high-frequency oscillations of the relative sea level lasting the 500kyrs carbonate deposition from Tonnerre, we suggest that the stratigraphic architecture of carbonate platforms in the Upper Oxfordian might be driven by glacio-eustatic sea-level changes. The succession of reef aggradation

and of lowstand erosion events indicated by this study perfectly fits with the concept of glacio-eustatism in icehouse mode. These new findings have important implications to improve knowledge on the Upper Jurassic climate. Cecca et al. (2005) recently mentioned that detailed paleoecological studies of peri-equatorial Oxfordian reefs are urgently needed for a more accurate time resolution of Oxfordian paleoclimatic changes. Our study strongly contributes to this topic and demonstrates that rapid paleoenvironmental changes occurred during the Upper Oxfordian and might be directly correlated with glacio-eustatic sea-level fluctuations.

Implications for imaging carbonate platforms using GPR

Regarding published works, penetration depths gained in this study (20m with a monostatic 200 MHz antenna) seem to be rather uncommon. Excepted the results gained by Asprion et al. (2009), such penetration depths seem to have never been reported hitherto within carbonate series for this prospecting frequency (200 MHz) compared to studies devoted to geological prospecting (25 to 100 MHz). Moreover, these results indicate a penetration depth at least equals to those gained with 25 to 100 MHz antennas in several studies devoted to carbonate facies (Pratt and Miall 1993, Grasmueck et al. 2004, Neal 2004), with a twice better resolution at least (vertical resolution is 25 cm here, with a 120 MHz return central frequency). In first approach, these important penetration depths for this prospecting frequency can be related to a pure carbonate setting (up to 100 % $CaCO_3$ content for the whole sequences, no clay within the bedding planes), and to a very reduced to non-existing top soil layer (i.e. GPR antennas were in direct contact with the cap rock), resulting in very few loss at the near-surface. The influence of this last parameter is clearly demonstrated at the beginning of the P1 profile (Fig. 7), where the presence of a thin top soil layer strongly attenuates the GPR response. It can be noted that these penetration depths are comparable to those obtained by several works devoted to the study of fractures located within urgonian limestone cliffs of SE France (Jeannin et al., 2006; Deparis et al., 2007). These particular prospections were generally conducted on top of a cliff, perpendicular to the bedding planes, with unshielded antennas. Excepted for the antennas which loose less energy when unshielded, the absence of soil layer and clayey bedding plane (similar conditions in our study) can be considered as essential conditions for reaching a good

penetration depth, and, therefore, for elaborating the most accurate geological prediction when no outcrop exposures are available..

CONCLUSIONS

The successful high-resolution 2D GPR survey dedicated to reefal and peri-reefal Calcaire de Tonnerre Formation offers new insight into the spatial distribution of sedimentary features of a carbonate platform. It was possible to image the internal architecture of a complex coral reef system on a meter to plurimeter scale and to confirm the relationships that exist between the growth of Upper Jurassic coral reefs and topographic highs. The integration of sedimentological and geophysical approaches clearly demonstrates its efficiency to improve a sedimentological model where no outcrop exposures are available.

The sedimentological study confirms that Upper Jurassic corals were able to adapt themselves to different environmental conditions and to respond quickly to both a major change in sedimentation rate and/or a relative sea-level oscillation. This major biological adaptation to rapid environmental changes explains why Upper Jurassic corals were widely developed on pericontinental and epeiric Tethyan seas, from Russia to Rumania through Poland, Germany, Switzerland, Eastern France, Eastern Spain, Southern Portugal to Texas and New Mexico. The study of the carbonate platform from Tonnerre provides an outstanding example for Upper Jurassic reefs that illustrates the response of coral reefs to rapid environmental changes, and the progressive evolution of the depositional profile showing the constant interplay among carbonate production, associated sedimentary facies, variations in accommodation, and erosional events.

This work presents an observation scale that perfectly fits between outcrop scale (some meters to some tens of meters) and seismic scale (several hundreds of meters to some kilometers). Expanding this 2D feasibility study into 3D data acquisition would allow a more comprehensive characterization, in particular to better anticipate the important lateral changes of facies.

ACKNOWLEDGEMENTS

The authors dedicate this work to Jean-Paul Loreau (1940-2004), Professor of Geology at the University of Burgundy and Director of the Earth Sciences Department of

Dijon. We would like to thank Milan Berès (University of Geneva) for his help in geophysical processing of our data. We express our gratitude to Luis Pomar (University of Balearic Islands), Guy Cabioch (IRD Nouméa) and Elias Samankassou (University of Geneva) for their suggestions and comments on the sedimentological study.

REFERENCES

Asprion, U. and **Aigner, T.** (1999) Towards realistic aquifer models: three-dimensional georadar surveys of quaternary gravel deltas (Singen Basin, SW-Germany). *Sed. Geol.*, **129**, 281-297.

Asprion, U. and **Aigner, T.** (2000) An initial attempt to map carbonate buildups using ground-penetrating radar: an example from the Upper Jurassic of SW Germany. *Facies*, **42**, 245-252.

Asprion, U.; Westphal, H.; Nieman, M. and **Pomar, L**. (2009) Extrapolation of depositional geometries of the Menorcan Miocene carbonate ramp with ground-penetrating radar. *Facies,* **55**(1), 37-46.

Beauvais, L. (1973) Upper Jurassic hermatypic corals. In: *Atlas of palaeobiogeography* (Ed. A. Hallam) Elsevier, Amsterdam.

Beres, M., Green, A. G., Huggenberger, P. and **Horstmeyer, H.** (1995) Mapping the architecture of glaciofluvial sediments with three-dimensional georadar. *Geology*, **23** (12), 1087-1090.

Beres, M. and **Haeni, F. P.** (1991) Application of ground-penetrating-radar methods in hydrogeologic studies. *Ground Water*, **29**, 375-386.

Beres, M., Huggenberger, P., Green, A. G. and **Horstmeyer, H.** (1999) Using two- and three-dimensional georadar methods to characterize glaciofluvial architecture. *Sed. Geol.*, **129**, 1-24.

Berner, R.A. (1994) Geocarb II: a revised model of the atmospheric CO2 over Phanerozoic time. *Am. J. Sci.*, **294**, 56-91.

Bertling, M. and **Insalaco, E.** (1998) Late Jurassic coral/microbial reefs from the northern Paris Basin: Facies, Palaeoecology and Palaeogeography. *Palaeogeogr. Palaeoclim. Palaeoecol.*, **139**, 139-175.

Cecca, F., Lathuilière, B., Marchand, D., Gardin, S. and **Bartolini, A.** (2001) Enregistrements paléobiologique et paléoécologique de fluctuations paléoclimatiques à l'Oxfordien (Jurassique supérieur). *Séance Sp. Géol. Fr.*, 19-21.

Cecca, F., Martin Garin, B., Marchand, D., Lathuiliere, B. and **Bartolini, A.** (2005) Paleoclimatic control of biogeographic and sedimentary events in Tethyan and peri-Tethyan areas during the Oxfordian (Late Jurassic). *Palaeogeogr. Palaeoclim. Palaeoecol.*, **222**, 10-32.

Chevalier, F., Garcia, J.P., Quesne, D., Guiraud, M. and **Menot, J.C.** (2001) Corrélations et interprétations génétiques dans les formations récifales oxfordiennes de la haute vallée de l'Yonne (sud-est du Bassin de Paris, France). *Bull. Soc. Geol. Fr.*, **172**, 69-84.

Collins, M.E., Cum, M. and **Haenninen, P.** (1994) Using ground-penetrating radar to investigate a subsurface karst landscape in north-central Florida. *Geoderma*, **61**, 1-15.

Crevello, P. and **Harris, P.M.** (1982) Depositional models for Jurassic reefal build-ups. Proc. Gulf Coast Sect. SEPM, 3rd An. Res. Conf., pp. 57-101.

Dagallier, G., Laitinen, A. I., Malartre, F., Van Campenhout, I. P. A. M. and **Veeken, P. C. H.** (2000) Ground penetrating radar application in a shallow marine Oxfordian limestone sequence located on the eastern flank of the Paris basin, NE France. *Sed. Geol.*, **130**, 149-165.

Daniels, D. J. (1996) Surface-penetrating radar. The Institution of Electrical Engineers, London, UK, 300 pp.

Deparis, J., Garambois, S. and **Hantz, D.** (2007) On the potential of ground penetrating radar to help rock fall hazard assessment: A case study of a limestone slab, gorges de la Bourne (French Alps). *Eng. Geol.*, **94**, 89-102.

Dromart, G., Garcia, J.P., Picard, S., Atrops, F., Lecuyer, C. and **Sheppard, S.M.F.** (2003) Ice age at the Middle/Late Jurassic transition? *Earth Planet. Sci. Lett.*, **213**, 205-220.

Droxler, A. W., Morse, J.W. and **Kornicker, W.A.** (1988) Controls on carbonate mineral accumulation in Bahamian basins and adjacent Atlantic Ocean sediments. *J. Sed. Petrol.*, **11**, 120-130.

Dupraz, C. (1999) Paléontologie, paléoécologie et évolution des faciès récifaux de l'Oxfordien moyen-supérieur (Jura suisse et français). *GeoFocus*, **2**, 1-200.

Dupraz, C. and **Strasser, A.** (2002) Nutritional modes in coral-microbialite reefs (Jurassic, Oxfordian, Switzerland); Evolution of trophic structure as a response to environmental change. *Palaios*, **17**, 449-471.

Ellis, P.M., Wilson, R.C.L. and **Leinfelder, R.R.** (1990) Controls on Upper Jurassic carbonate buildup development in the Lusitanian Basin, Portugal. In : *Carbonate Platforms; facies, sequences and evolution* (Eds. M.E. Tucker, J.L. Wilson, P.D. Crevello, J.R. Sarg, J.F. Read), *Int. Ass. Sediment. Spec. Publ.,* 9, Oxford, 169-202.

Gaillard, C. (1983) Les biohermes à spongiaires et leur environnements dans l'Oxfordien du Jura Méridional. *Doc. Lab. Géol. Fac. Sci. Lyon*, **90**, 1-515.

Goutaland, D., Winiarski, T., Dubé, J.-S., Bièvre, G., Buoncristiani, J.-F., Chouteau, M. and **Giroux, B.** (2008) Hydrostratigraphic characterization of glaciofluvial deposits underlying an infiltration basin using ground-penetrating radar. *Vadose Zone Journal*, **7** (1), 1-14.

Grasmueck, M. and **Weger, R.** (2002) 3D GPR reveals complex internal structure of Pleistocene oolitic sandbar. *Lead. Edge*, **21**, 634-639.

Grasmueck M., Weger R. and **Horstmeyer, H.** (2004) Three-dimensional ground-penetrating radar imaging of sedimentary structures, fractures and archaeological features at submeter resolution. *Geology*, **32**, 933-936.

Gröcke, D.R., Price, G.D., Ruffell, A.H., Mutterlose, J. and **Baraboshkin, E.** (2003) Isotopic evidence for Late Jurassic–Early Cretaceous climate change. *Palaeogeogr. Palaeoclim. Palaeoecol.*, **202**, 97-118.

Gygi, R.A. (1986) Eustatic sea level changes of the Oxfordian (Late Jurassic) and their effects documented in sediments and fossil assemblages of an epicontinental sea. *Eclog. Geol. Helvet.*, **79**, 455-491.

Gygi, R.A. and **Persoz, F.** (1986) Mineralostratigraphy, litho- and biostratigraphy combined in correlation of the Oxfordian (Late Jurassic) formations of the Swiss Jura range. *Eclog. Geol. Helvet.*, **79**, 385-454.

Haq, B.U., Hardenbol, X. and **Vail, Y.** (1988) Mesozoic and Cenozoic chronostratigraphy and cycles of sea-level change. In : *Sea level changes, an integrated approach* (Eds. C.K. Wilgus, B.S. Hastings, C.A. Ross, H. Posamentier, J. Van-Wagoner and C.G. Kendall), *SEPM Spec. Pub.*, 42, 72-108.

Heinz, J. and **Aigner, T.** (2003) Three-dimensional GPR analysis of various Quaternary gravel-bed braided river deposits (southwestern Germany). In: *Ground Penetrating Radar in Sediments* (Eds C. Bristow and H. Jol), *Geol. Soc. Spec. Publ.,* London, **211**, 99-110.

Helm, C. and **Schülke, I.** (1998) A coral-microbialite patch-reef from the Late Jurassic (florigemma-Bank, Oxfordian) of NW Germany (Süntel Mountains). *Facies*, **39**, 75-104.

Hoffman A., Gruszczynski M., Malkowski K., Halas S., Matyja B.A. and **Wierzbowski A.** (1991) Carbon and oxygen isotope curves for the Oxfordian of central Poland. *Acta Geol. Pol.*, **43**, 157-164.

Hornung, J. and **Aigner, T.** (2002) Reservoir architecture in a terminal alluvial plain: an outcrop analogue study (Upper Triassic, Southern Germany) PartII: cyclicity, controls and models. *J. Petrol. Geol.*, **25**, 151-178.

Huggenberger, P. and **Regli, C.** (2006) A sedimentological model to characterize braided river deposits for hydrogeological applications. In: *Braided Rivers : Process, Deposits, Ecology and Management* (Eds. G. H. Sambrook-Smith, J. L. Best, C. S. Bristow, et al.), *Blackwell Publ.*, Oxford, UK, 51-74.

Insalaco, E. (1996) Upper Jurassic microsolenid biostromes of northern and central Europe: facies and depositional environment. *Palaeogeogr. Palaeoclim. Palaeoecol.*, **121**, 169-194.

Insalaco, E., Hallam, A. and **Rosen, B.** (1997) Oxfordian (Upper Jurassic) coral reefs in western Europe : reefs types and conceptual depositional model. *Sedimentology*, **44**, 707-734.

Jeannin, M., Garambois, S., Grégoire, C. and **Jongmans, D.** (2006) Multiconfiguration GPR measurements for geometric fracture characterization in limestone cliffs (Alps). *Geophysics*, **71**, 3, B85-B92.

Jansa, L.F. (1986) Paleoceanography and evolution of the North Atlantic Ocean Basin during the Late Jurassic. In : *The geology of North America* (Eds. P.R. Vogt, B.E. Tucholke), *Geol. Soc. Am.*, Boulder, USA, 603-616.

Jorry, S.J., Davaud, E. and **Caline, B.** (2003) The Nummulites Eocene Carbonates (central Tunisia and NE Libya): Sedimentology, depositional environment, and application to oil reservoirs. *J. Petrol. Geol.*, **26**, 283-306.

Kendall, C.G.C. and **Schlager, W.** (1981) Carbonates and relative changes in sea level. *Mar. Geol.*, **44**, 181-212.

Lambert, J. (1893) Etude stratigraphique sur le calcaire Séquanien de Tonnerre. *Mém. Soc. Paléont. Suisse*, **20**, 175-213.

Leinfelder, R.R. (1987) Formation and significance of Black Pebbles from the Ota Limestone (Upper jurassic, Portugal). *Facies*, **17**, 159-170.

Leinfelder, R.R. (1989) Intrabecken-Karbonatplattformen und Riffstrukturen im Ostteil des Lusitanischen Beckens – Fallbeispiele aus dem Oberjura von Portugal. Habilitation Thesis, University of Mainz, Germany.

Leinfelder, R.R. (1992) A modern-type Kimmeridgian reef (Ota Limestone, Portugal); implications for Jurassic reef models. *Facies*, **26**, 11-34.

Leinfelder, R.R. (1993) Upper Jurassic reef types and controlling factors. *Profil*, **5**, 1-45.

Leinfelder, R.R. (1994) Karbonatplattformen und Korallenriffe innerhalb siliziklastischer sedimentationsbereiche (Oberjura, Lusitanisches Becken, Portugal). *Profil*, **6**, 1-207.

Leinfelder, R.R. (2001) Jurassic reef ecosystem. In: *The history and sedimentology of ancient reef systems* (Ed. J.D. Jr Stanley), *Kluwer Academic/Plenum Publishers*, New York, 251-309.

Leinfelder, R.R., Krautter, M., Laternser, R., Nose, M., Schmid, D., Scheigert, G., Werner, W., Keupp, H., Brugger, H., Herrmann, R., Rehfeld-Kiefer, U., Schroeder, R., Reinhold, C., Knock, R., Zeiss, A., Schweizer, V., Christmann, H., Menges, G. and **Luterbacher, H.** (1994) The origin of Jurassic reefs : current research developments and results. *Facies*, **31**, 1-56.

Loreau, J.-P. (1967) La Pierre de Tonnerre : Etude stratigraphique et pétrographique dans le Jurassique supérieur du tonnerrois. DES Paris, 80 p.

Loreau, J.-P. (1975) Les grands traits de la sédimentation sur l'emplacement de l'actuelle bordure sud-est du Bassin de Paris au Jurassique supérieur. IXme Congrès Int. Sédimentologie, Nice, pp. 273-281.

Loreau, J.-P. (1979) Nature calcitique initiale et diagenèse des oolithes jurassiques du Bassin de Paris. *Ass. Sédiment. Fr. Spec. Publ.*, **1**, 417-429.

Loreau, J.-P. (1982) Sédiments aragonitiques et leur genèse. *Mém. Muséum Hist. Nat. Paris*, série C, **47**, 312 p.

Loreau, J.-P. and **Tintant, H.** (1968) Le calcaire de Tonnerre et les formations adjacentes du Jurassique supérieur de l'Yonne: Observations stratigraphiques et paléontologiques. *Bull. Soc. Géol. Fr.*, **X7**, 341-357.

Loreau, J.P., Alabouvette, B., Mégnien, C., Mégnien, F. and **Thierry, J.** (1970) Tonnerre. In: Carte géologique de la France à 1/50 000. BRGM, Orléans, France.

McMechan, G. A., Loucks, R. G., Zeng, X., and **Mescher, P.** (1998) Ground penetrating radar imaging of a collapsed paleocave system in the ellenburger dolomite, central texas. *J. App. Geophy.*, **39**, 1-10.

Menot, J.C. (1974) Sur l'organisation du système récifale inférieur Oxfordien aux confins de l'Yonne et de la Nièvre. *C. R. Acad. Sci.*, **278**, 1459-1462.

Menot, J.C. (1980) Formations récifales du Jurassique Supérieur de la vallée de l'Yonne. *Geobios Mém. Spéc.*, **4**, 47-53.

Menot, J.C. and **Rat, P**. (1967) Sur la structure du complexe récifal jurassique supérieur de la vallée de l'Yonne. *C. R. Acad. Sci.*, **264**, 2620-2623.

Meschede M., Asprion U. and **Reicherter, K**. (1997) Visualisation of tectonic structures in shallow-depth high-resolution ground-penetrating radar (GPR) profiles. *Terra Nova*, **9**, 167-170.

Moore, G.T., Hayashida, D.N., Ross, C.A. and **Jacobson, S.R**. (1992a) Paleoclimate of the Kimmeridgian/Tithonian (Late Jurassic) world: I. Results using a general circulation model. *Palaeogeogr. Palaeoclimatol. Palaeoecol.*, **93**, 113-150.

Moore, G.T., Sloan, L.C., Hayashida, D.N. and **Umaigar, N.P**. (1992b) Paleoclimate of the Kimmeridgian/Tithonian (Late Jurassic) world: II. Sensitivity tests comparing three different paleotopographic settings. *Palaeogeogr. Palaeoclimatol. Palaeoecol.*, **95**, 229-252.

Müller, G. and **Gastner, M**. (1971) The "karbonat-bombe", a simple device for the determination of the carbonate content in sediments, soils and other materials. **Neus Jahrbuch Fuer Mineralogie**, *10*, 466-469.

Mutti, E. and **Normak, W. R.** (1987) Comparing exemples of modern and anciant turbidite systems: problems and concepts. In: Leggett, J. K., Zuffa, G. G. (Eds.), *Marine clastic sedimentology. Concepts and case studies. Graham & Trotman Publishing*, London, pp. 1-38.

Mutti, E. and **Normark, W. R**. (1991) An integrated approach to study of turbidite systems. In: Seismic facies and sedimentary processes of submarine fans and turbidite systems. pp. 75-105.

Neal, A. (2004). Ground-penetrating radar and its use in sedimentology: principles, problems and progress. *Earth-Sci. Rev.*, **66**, 261-330.

Olivier, N., Carpentier, C., Martin-Guérin, B., Lathuilière, B., Gaillard, C., Ferry, S., Hantzpergue, P. and **Geister, J**. (2004) Coral-microbialite reefs in pure carbonate versus mixed carbonate-siliciclastic depositional environments; the example of the Pagny-sur-Meuse section (upper Jurassic, northeastern France). **Facies**, *50*, 229-255.

Olivier, N., Hantzpergue, P., Gaillard, C., Pittet, B., Leinfelder, R., Schmid, D.U. and **Werner, W**. (2003) Microbialite morphology, structure and growth: a model of the Upper Jurassic reefs of the Chay Peninsula (western France). *Palaeogeogr. Palaeoclim. Palaeoecol.*, **193**, 383-404.

Oschmann, W. (1988) Kimmeridge clay sedimentation – a new cycli model. *Palaeogeogr. Palaeoclim. Palaeoecol.*, **65**, 313-332.

Oschmann, W. (1990) Environmental cycles in the late Jurassic northwest European epeiric basin; interaction with atmospheric and hydrospheric circulations. In : Aigner, T., Dott, R.H. (Eds.), *Processes and patterns in epeiric basin. Sed. Geol.* **69**, pp 331-332.

Pittet, B. (1996) Contrôles climatiques, eustatiques et tectoniques sur des systèmes mixtes carbonatés/siliciclastiques de plate-forme : exemple de l'Oxfordien (Jura Suisse, Normandie, Espagne). Ph.D. Thesis, Fribourg University, Switzerland.

Pittet, B. and **Strasser, A**. (1998) Long-distance correlations by sequence stratigraphy and cyclostratigraphy : examples and implications (Oxfordian from the Swiss Jura, Spain, and Normandy). *Geol. Rund.*, **86**, 852-874.

Pittet, B., Strasser, A. and **Mattioli, E**. (2000) Depositional sequences in deep-shelf environments : a response to sea level changes and shallow-platform carbonate productivity (Oxfordian, Germany and Spain). *J. Sed. Res.*, **73**, 392-407.

Pratt B.R. and **Miall, A.D**., 1993. Anatomy of a bioclastic grainstone megashoal (Middle Silurian, southern Ontario) revealed by ground-penetrating radar. *Geology*, **21**, 223-226.

Price, G. and **Gröcke, D.R**. (2002) Strontium-isotope stratigraphy and oxygen- and carbon-isotope variation during the Middle Jurassic– Early Cretaceous of the Falkland Plateau, South Atlantic. *Palaeogeogr. Palaeoclim. Palaeoecol.*, **183**, 209-222.

Price, G. and **Sellwood, B.W**. (1997) "Warm" palaeotemperatures from high Late Jurassic palaeolatitudes (Falkland Plateau): ecological, environmental or diagenetic controls? *Palaeogeogr. Palaeoclim Palaeoecol.*, **129**, 315-327.

Pringle, J.K., Westerman, A.R., Clark, J.D., Drinkwater, N.J. and **Gardiner, A.R**. (2004) 3D high-resolution digital models of outcrop analogue study sites to constrain reservoir model uncertainty: an example from Alport Castles, Derbyshire, *UK. Petrol. Geosci*., **10**, 343-352.

Reppert, P. M., Dale Morgan, F. and **Toksöz, M. N**. (2000) Dielectric constant determination using ground-penetrating radar reflection coefficients. *J. Appl. Geophy.*, **43**, 189-197.

Ross, C.A., Moore, G.T. and **Hayashida, D.N**. (1992) Late Jurassic paleoclimate simulation-paleoecological implications for Ammonoid provinciality. *Palaios,* **7**, 487-507.

Sandmeier, K. J. (2007) Reflexw 4.5 user guide. Sandmeier Scientific Softwares, Karlsruhe, Germany.

Schmid, D.U. (1996) Marine Mikrobolithe und Mikroinkrustierer aus dem Oberjura. *Profil*, **9**, 101-251.

Sellwood, B.W. and **Valdes, P.J**. (1997) Geological evaluation of climate General Circulation Models and model implications. *Terra Nova,* **9**, 75-78.

Sellwood, B.W., Valdes, P.J. and **Price, G.D**. (2000) Geological evaluation of multiple general circulation model simulations of Late Jurassic palaeoclimate. *Palaeogeogr. Palaeoclim. Palaeoecol*., **156**, 147-160.

Sigurdsson, T. and **Overgaard, T**. (1998) Application of gpr for 3-d vizualisation of geological and structural variation in a limestone formation. *J. Appl. Geophy*., **40**, 29-36.

Strasser, A., Aurell, M., Bádenas, B., Meléndez, G. and **Tomás, S**. (2005) From platform to basin to swell: orbital control on sedimentary sequences in the Oxfordian, Spain. *Terra Nova*, **17**, 407-413.

Sun, S. Q. and **Wright, V. P**. (1998) Controls on reservoir quality of an upper jurassic reef mound in the palmers wood field area, weald basin, southern england. *AAPG Bulletin*, **82** (3), 497-515.

Valdes, P.J. and **Sellwood, B.W**. (1992) A paleoclimate model for the Kimmeridgian. *Palaeogeogr. Palaeoclim. Palaeoecol.*, **95**, 47-72.

Veizer, J.Y., Goddéris, Y. and **Francois, L.M**. (2000) Evidence for decoupling of atmospheric CO2 and global climate during the Phanerozoic eon. *Nature*, **408**, 698-701.

Vogt, P.R. and **Tucholke, B.R**. (1986) Perspective on the geology of the North Atlantic Ocean. In : Vogt, P.R., Tucholke, B.E. (Eds.), *The geology of North America. Geol. Soc. Am*., Boulder, CO, USA, pp 1-18.

Werner, W., Leinfelder, R.R., Fürsich, F.T. and **Krautter, M.** (1994) Comparative palaeoecology of marly coralline sponge-bearing reefal associations from the Kimmeridgian (Upper Jurassic) of Portugal and southwestern Germany. *Cour. Forsch.-Inst. Senckenb*., **172**, 381-397.

Wierzbowski, H. (2002) Detailed oxygen and carbon isotope stratigraphy of the Oxfordian in Central Poland. *Int. J. Earth Sci*., **91**, 304-314.

Wierzbowski, H. (2004) Carbon and oxygen isotope composition of Oxfordian–Early Kimmeridgian belemnite rostra: palaeoenvironmental implications for Late Jurassic seas. *Palaeogeogr. Palaeoclim. Palaeoecol*., **203**, 153-168.

Ziegler, P.A. (1988) Evolution of the Artic-North-Atlantic and the western Tethys. *AAPG Mem.*, **43**, 198 pp.

TABLE CAPTION

Process	Goal	Parameters (when applicable)
Enhance signals		
Stack	Remove high frequency noise	4 traces
Time zero correction	Align traces to same origin in time	Alignment of direct waves
Dewow	Remove low-frequency system-dependent noise	350 ns
Background removal	Remove constant temporal noise	350 ns
Bandpass filtering	Remove low and high frequency	LCO/LP/UP/OCO: 50/100/150/225
Gain correction	Compense EM energy attenuation with time	Energy decay
Geometry calibration		
Migration	Time to depth conversion	0,12 m/ns
Topography correction	Reflect the true topography	D-GPS calibration each 10 m

Table 01: GPR data processing sequence concerning the 200 MHz antenna. LCO: lower cut-off frequency, LP: lower plateau frequency, UP: upper plateau frequency, UCO: upper cut-off frequency.

Sample	Facies	$CaCO_3$ (%)	Permeability (mD)	Porosity (%)
Ton2	P.F.F.	100	5,07	9,15
Ton2''	P.F.F.	100	24,22	19,27
Ton3	L.C.P.R.	100	23,09	26,43
Ton3'	L.C.P.R.	100	37,6	18,54
Ton5	M.C.F.	100	2,31	17,21

Table 02: Petrophysical measurements made on plugged samples. The location of samples on outcrop DEV1 is reported on Figure 6. P.F.F.: Prograding flanked facies; L.C.P.R.: Lamellar-coral patch reef; M.C.F.: Muddy channeling facies.

FIGURE CAPTION

Figure 1: Jurassic paleogeography of the Atlantic region (after Vogt and Tucholke, 1986) and the Northern Tethys domain (modified after Leinfelder 1987; Ziegler, 1988; Leinfelder, 1989; Ellis et al., 1990), and possible oceanic circulation pattern (modified after Oschmann, 1988, 1990; Jansa, 1986; Leinfelder, 1992, 1994). During this interval, the distribution of carbonate platforms widely extended along both margins of Atlantic and northern Tethys Oceans.

Figure 2: Location and geology of the study area. A: Location of the study area in France. B: Geological map of the study area (after Loreau et al., 1970) with location of the studied outcrops. Coordinates are in meters according to French Lambert projection. C: Biostratigraphic framework and relative sea-level fluctuations of the Upper Oxfordian. The stratigraphic succession of the ammonite zones is classically defined as a standard zonation for the sub-Mediterranean province (Insalacco 1996). Ages at boundaries of ammonite zone have been integrated from Strasser et al. (2005).

Figure 3: Location of outcrops (DEV1 and DEV2) and of GPR profiles (P1, P2 and P3).

Figure 4: Evidence of coral-dominated reefs and off-reef bioclastic deposits in the Calcaire de Tonnerre Formation. A: Panorama of the DEV1 outcrop located along the roadcut of Tonnerre and geometries of coral reefs and of prograding wedges. The location of discontinuous boundaries is based on lateral bedding terminations (onlap, downlap and

erosion top). B: Panorama of the DEV2 outcrop (facing DEV1) and geometries of coral reefs and of prograding wedges. C: Correlation between two synthetic sections logged through the R1-R3 reefs from both DEV1 and DEV2 outcrops. Section 1 shows two superimposed coral-dominated reef units, while inter-reef grainstones are intercalated between reefs on section 2. Facies f1: dish coral-dominated reef facies; Facies f2: bioclastic grainstones containing coral rubble, skeletal debris and peloids; Facies f3: branching coral-dominated reef facies showing a well preserved Calamophylliopsis sp. coral in life position; Facies f4: mudstone/wackestone facies composed of scattered echinoid debris and other bioclasts. Abbreviations R1, R2, R3, R4, R5 and R6 represent coral-dominated patch reefs. DT1, DT2, DT3, DT4 and DT5 are unconformity surfaces.

Figure 5: Geometries of sedimentary packages in the Calcaire de Tonnerre Formation. A: Off-reef prograding facies. These progradations may reach metric heights. This detail also shows the pinching out of DT4 and DT5 erosive surfaces. B: Detail of the R6 patch reef at outcrop DEV2. The reef grew on a high energy, coral rubble facies containing metric blocks (marked by B) and shows a lenticular reef crest at its top. This branching coral-dominated reef is overlain by onlapping mudstones/wackestones (OF). Thickness of the outcrop is about 15m. C: Evidence of erosion (marked by unconformity DT4) affecting the top of the R3 reef at outcrop DEV1. The pacth reef is covered by downlapping packstones. Unconformity DT5 and facies of the next accretional unit are also visible. The location of the photographs is indicated on Figs. 4A and 4B.

Figure 6: Synthesis of the succession of depositional sequences, associated sedimentary packages and processes. The morphology of the depositional profile of the carbonate platform was dominantly controlled by allocyclic processes (variations of relative sea level) which induced major erosional events at sequence boundaries. High-frequency, moderate to low amplitude changes in relative sea level are detected at the Upper Oxfordian. Increase in accommodation space has triggered the edification of coral reefs.

Figure 7: Illustration of GPR profile P1 acquired on top of outcrop DEV1 (location on Fig. 3). A: Photomosaic and sedimentological interpretation of outcrop DEV1 (see Fig. 4 for details). B: Processed GPR profile P1. The location of plugged samples is indicated.

Figure 8: Examples of geometries detected on GPR profiles. A: GPR Detail on profil P1(200 MHz antenna) showing prograding and channel-fill depositional sequences; major erosive unconformities are clearly detected by pointing lateral reflector terminations. B: Illustration of small-scale channels on profil P2 (400 Mhz antenna); at outcrop, these channeling sequences are filling up with mudstones.

Figure 9: GPR facies and associated sedimentary facies. Location of close-ups is indicated on Fig. 7.

Figure 10: Interpretation of GPR profiles based on the definition of radar facies. A: Processed GPR profiles P1 (acquired on top of outcrop DEV1) and P3 (acquired at the base of outcrop DEV1), see Fig.3 for the location of both GPR surveys. B: Interpreted GPR profiles P1 and P3.

Figure 11: Synthetic sedimentological interpretation of outcrop DEV1 after the merge of GPR profiles P1 and P3. This allows the prolongation of major unconformities and the identification of the base of the coral reefs.

Figure 1

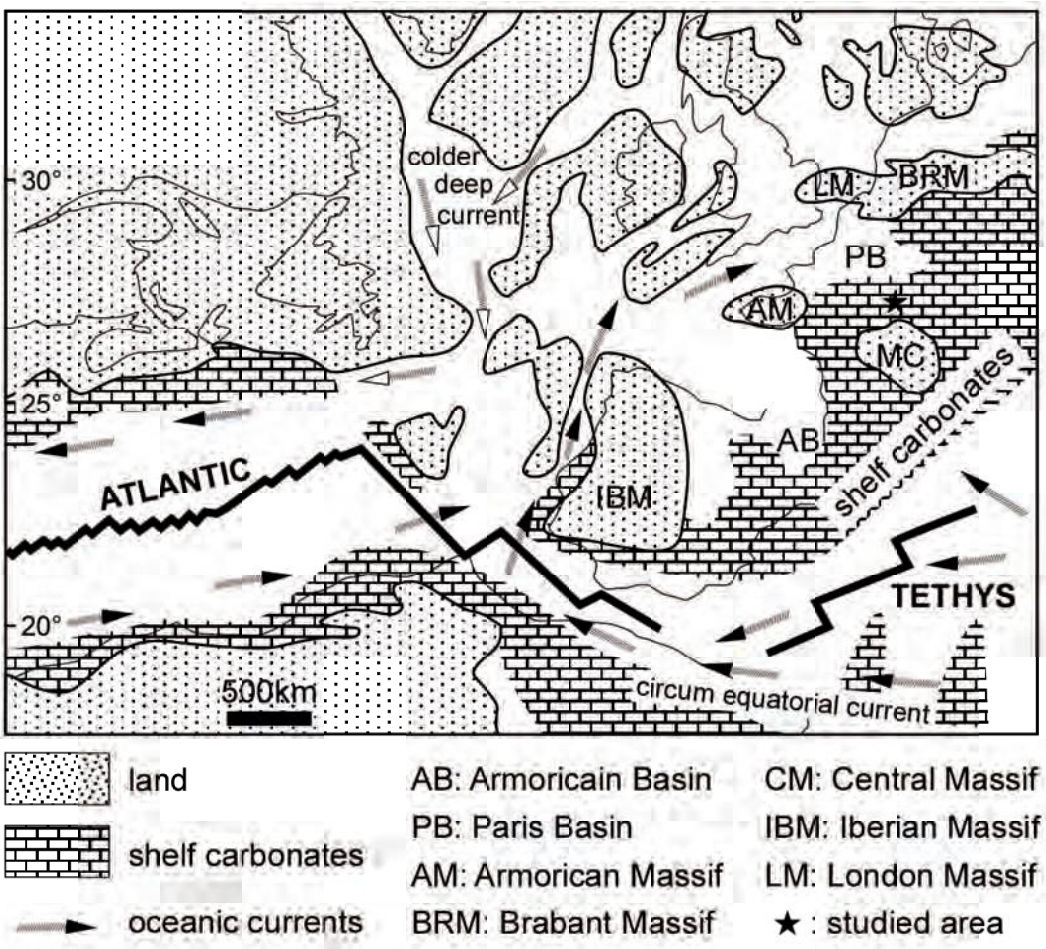
30°
25°
20°
colder
deep
current
LM
BRM
PB
AM
MC
AB
shelf carbonates
ATLANTIC
IBM
TETHYS
circum equatorial current
500km
land
shelf carbonates
oceanic currents
AB: Armoricain Basin
PB: Paris Basin
AM: Armorican Massif
BRM: Brabant Massif
CM: Central Massif
IBM: Iberian Massif
LM: London Massif
★ : studied area

Figure 2

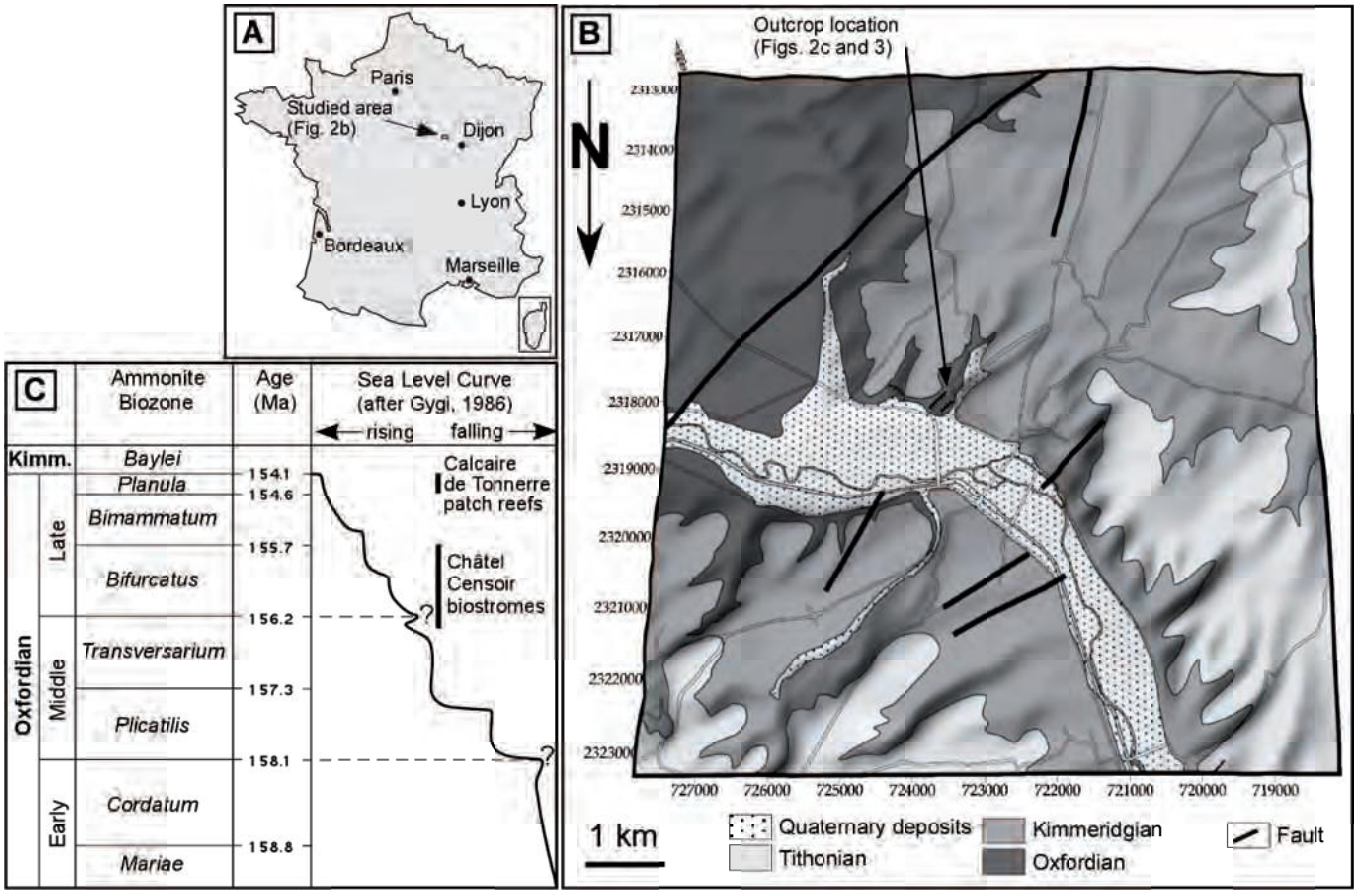
A
Paris
Studied area
(Fig. 2b)
Dijon
Lyon
Bordeaux
Marseille
B
Outcrop location
(Figs. 2c and 3)
N
2313000
2314000
2315000
2316000
2317000
2318000
2319000
2320000
2321000
2322000
2323000
727000
726000
725000
724000
723000
722000
721000
720000
719000
1 km
Quaternary deposits
Tithonian
Kimmeridgian
Oxfordian
Fault
C
Ammonite Biozone
Age (Ma)
Sea Level Curve (after Gygi, 1986)
rising
falling
Kimm.
Oxfordian
Late
Middle
Early
Baylei
Planula
Bimammatum
Bifurcatus
Transversarium
Plicatilis
Cordatum
Mariae
154.1
154.6
155.7
156.2
157.3
158.1
158.8
Calcaire de Tonnerre patch reefs
Châtel Censoir biostromes
?
?

Figure 3

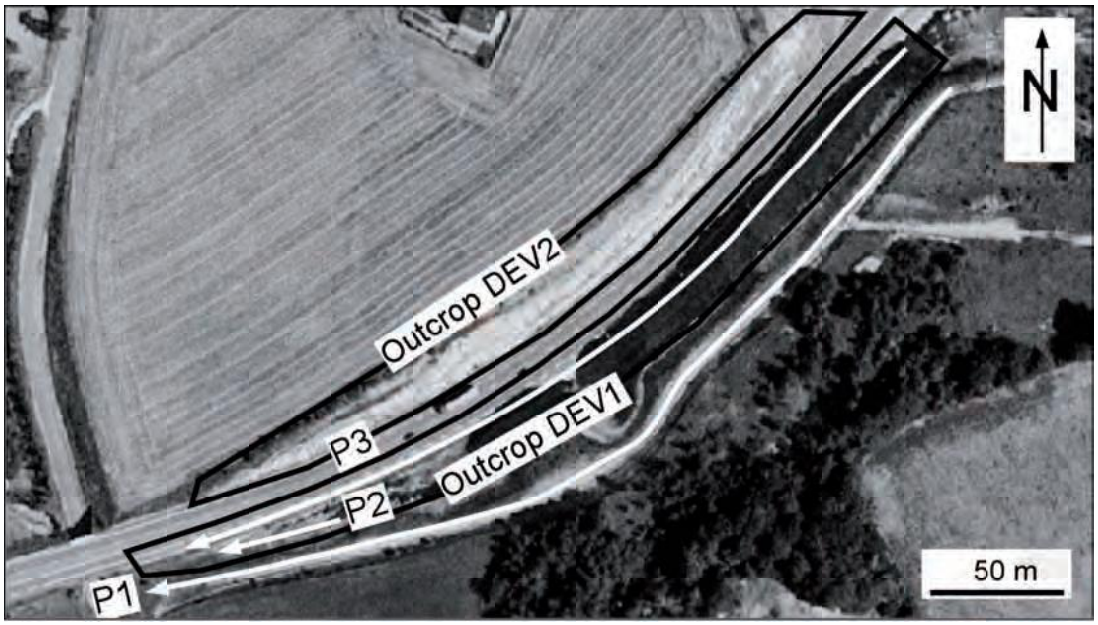

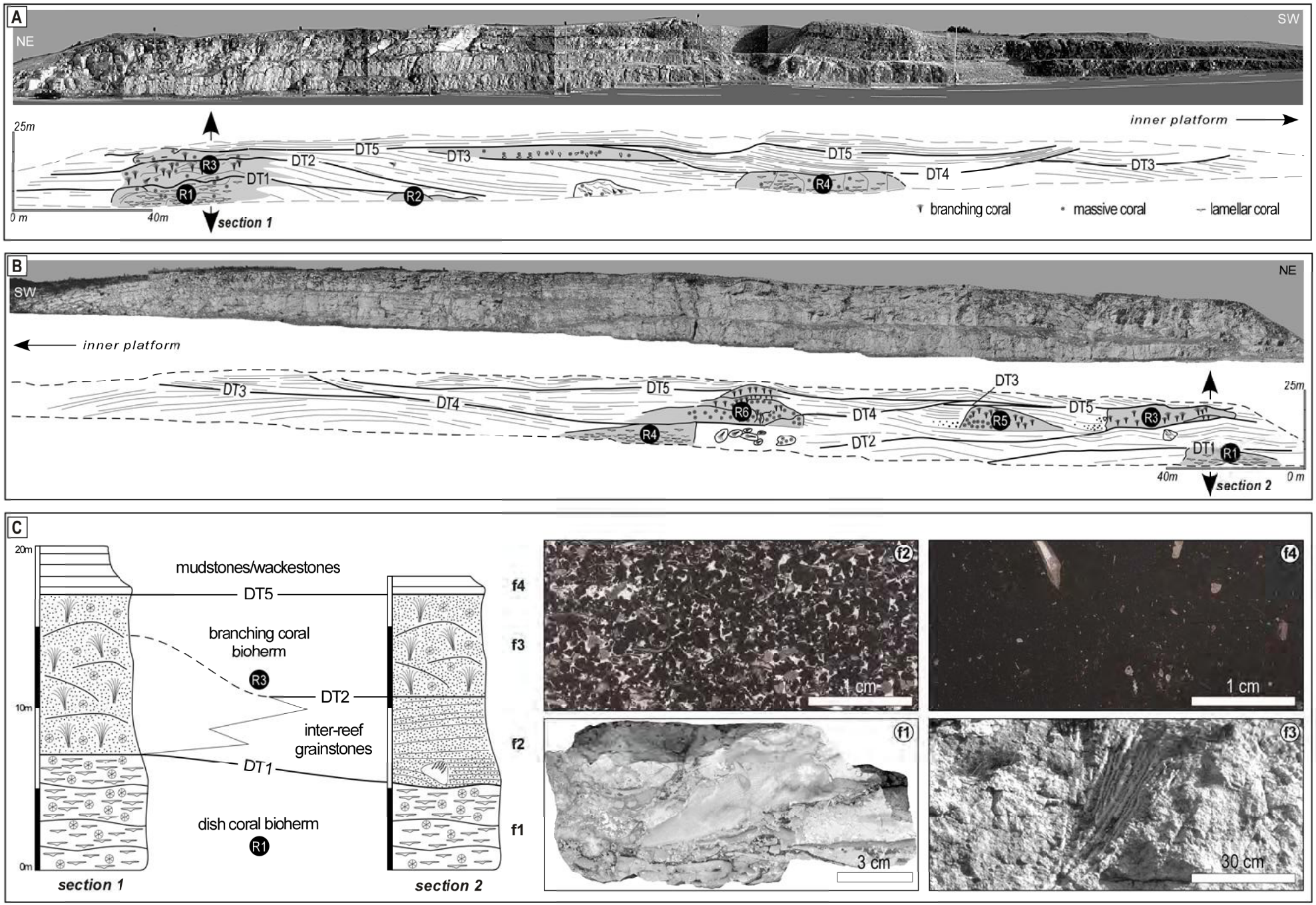
A
NE
SW
25m
inner platform
DT5
DT3
DT2
DT1
DT5
DT4
DT3
R3
R1
R2
R4
0 m
40m
section 1
branching coral
massive coral
lamellar coral
B
SW
NE
inner platform
DT3
DT4
DT5
DT3
DT4
DT5
DT2
DT1
R6
R4
R5
R3
R1
25m
40m
0 m
section 2
C
20m
10m
0m
mudstones/wackestones
DT5
branching coral bioherm
R3
DT2
inter-reef grainstones
DT1
dish coral bioherm
R1
section 1
section 2
f4
f3
f2
f1
f2
1 cm
f4
1 cm
f1
3 cm
f3
30 cm

Figure 4

Figure 5

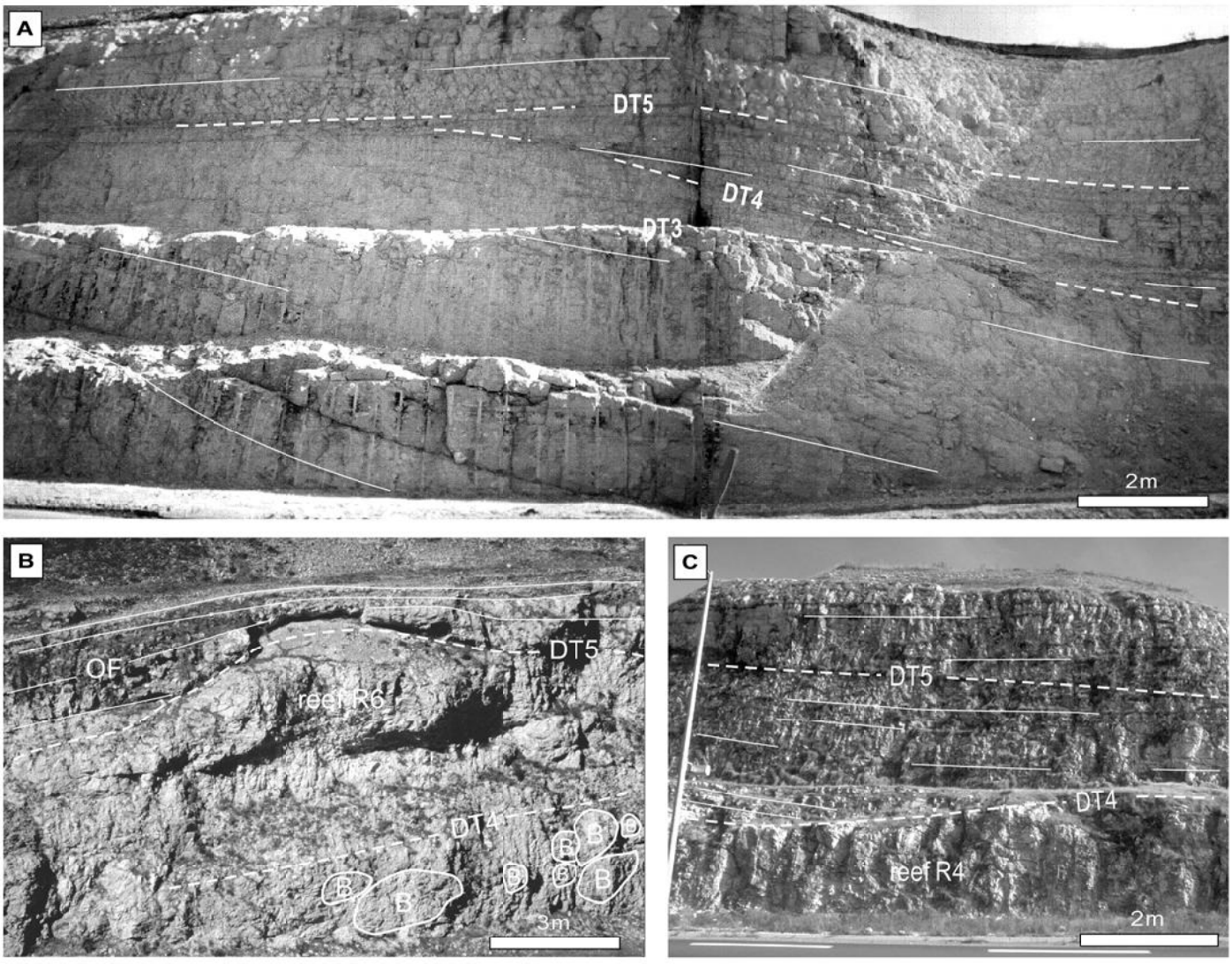

Figure 6

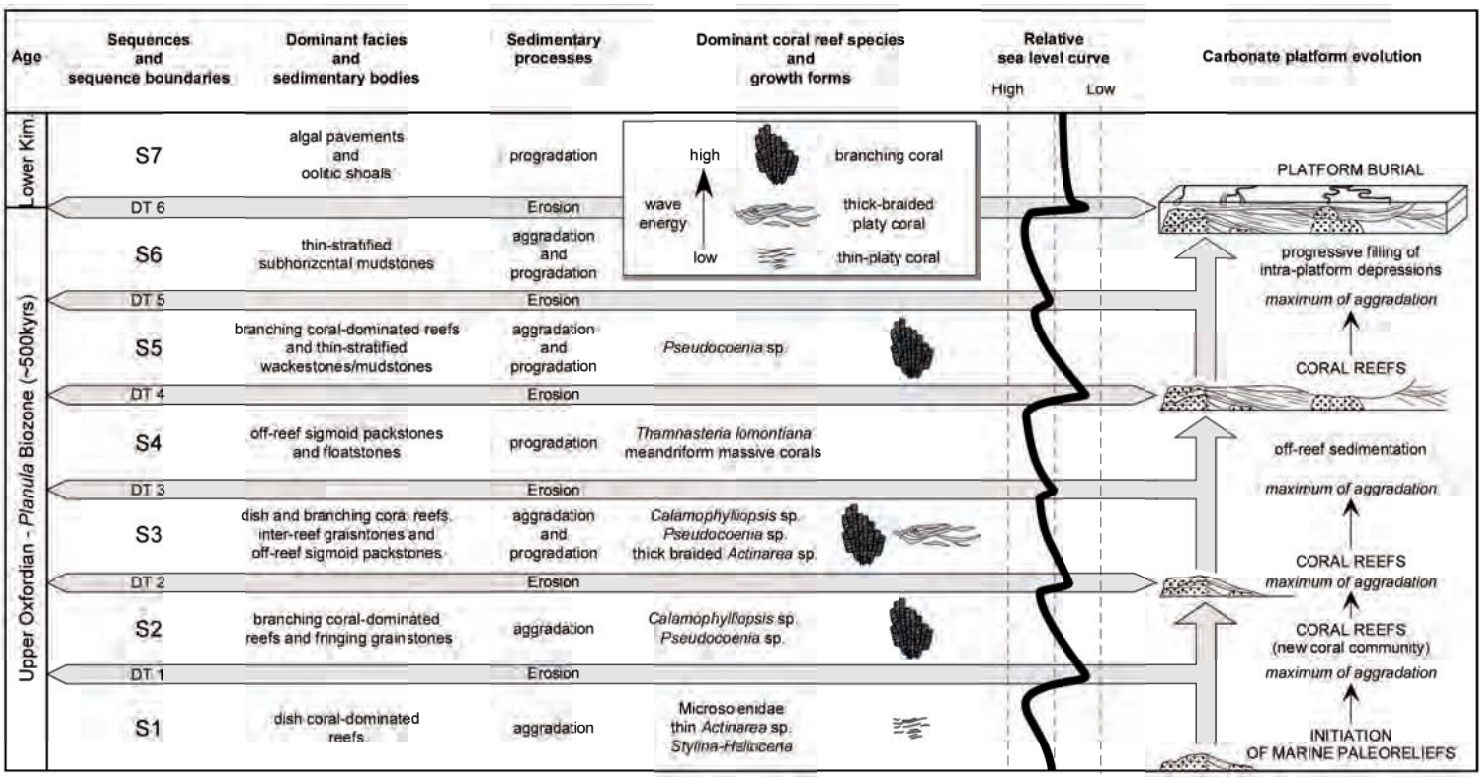
Age
Sequences and sequence boundaries
Dominant facies and sedimentary bodies
Sedimentary processes
Dominant coral reef species and growth forms
Relative sea level curve
High
Low
Carbonate platform evolution
Lower Kim.
Upper Oxfordian - Planula Biozone (~500kyrs)
S7
algal pavements and oolitic shoals
progradation
high
wave energy
low
branching coral
thick-braided platy coral
thin-platy coral
PLATFORM BURIAL
DT 6
Erosion
S6
thin-stratified subhorizontal mudstones
aggradation and progradation
progressive filling of intra-platform depressions
maximum of aggradation
DT 5
Erosion
S5
branching coral-dominated reefs and thin-stratified wackestones/mudstones
aggradation and progradation
Pseudocoenia sp.
CORAL REEFS
DT 4
Erosion
S4
off-reef sigmoid packstones and floatstones
progradation
Thamnasteria lomontiana meandriform massive corals
off-reef sedimentation
maximum of aggradation
DT 3
Erosion
S3
dish and branching coral reefs, inter-reef grainstones and off-reef sigmoid packstones
aggradation and progradation
Calamophylliopsis sp.
Pseudocoenia sp.
thick braided Actinarea sp.
CORAL REEFS
maximum of aggradation
DT 2
Erosion
S2
branching coral-dominated reefs and fringing grainstones
aggradation
Calamophylliopsis sp.
Pseudocoenia sp.
CORAL REEFS (new coral community)
maximum of aggradation
DT 1
Erosion
S1
dish coral-dominated reefs
aggradation
Microsolenidae
thin Actinarea sp.
Stylina-Heliocoenia
INITIATION OF MARINE PALEORELIEFS

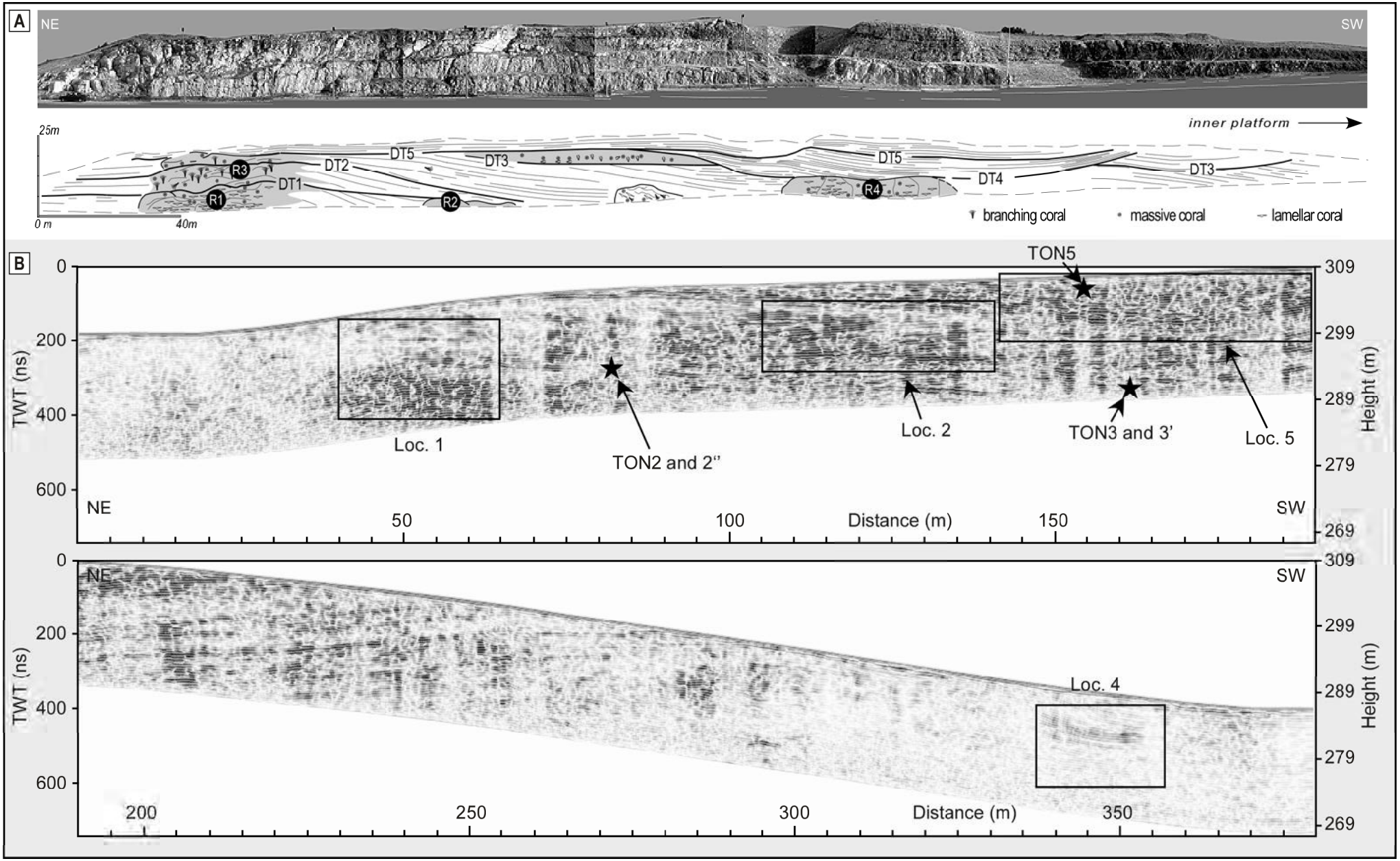
A
NE
SW
inner platform
25m
0 m
40m
DT1
DT2
DT3
DT4
DT5
R1
R2
R3
R4
branching coral
massive coral
lamellar coral
B
TON5
Loc. 1
TON2 and 2''
Loc. 2
TON3 and 3'
Loc. 5
Loc. 4
TWT (ns)
Height (m)
Distance (m)
NE
SW
0
200
400
600
309
299
289
279
269
50
100
150
200
250
300
350

Figure 7

Figure 8

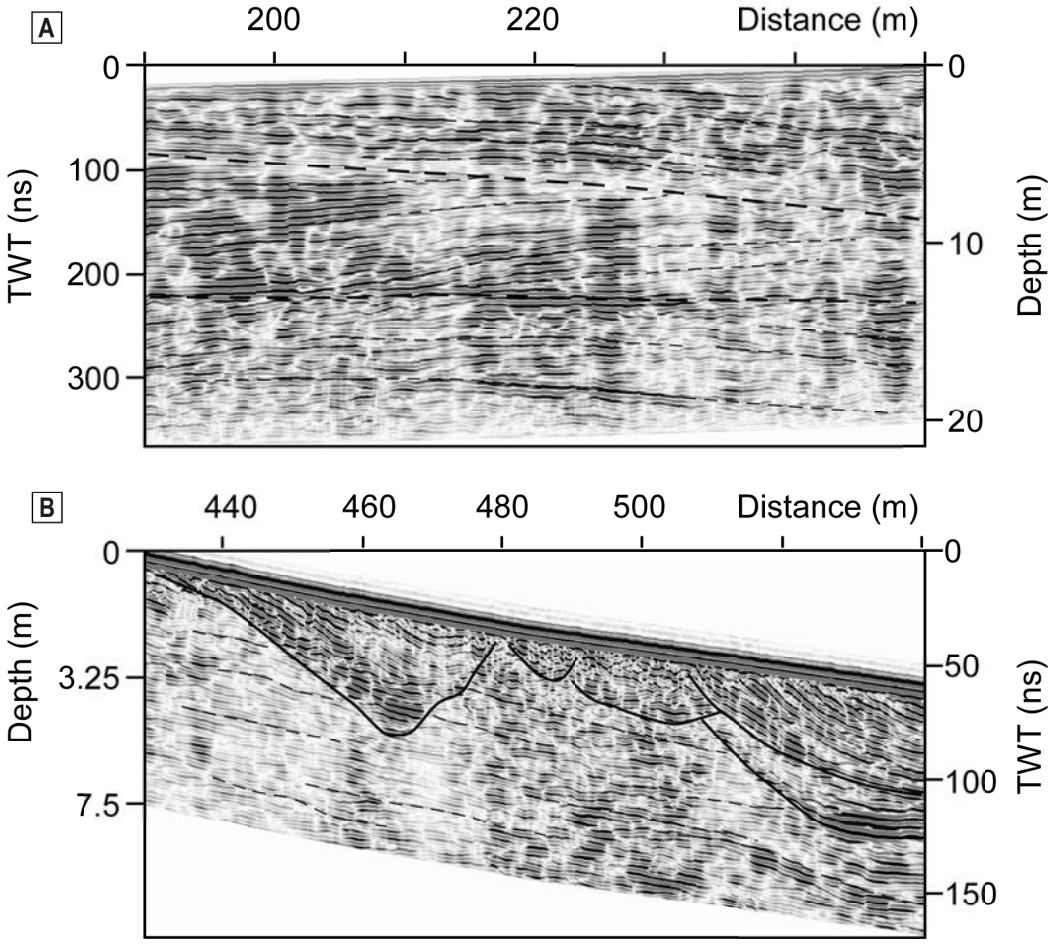
A
200
220
Distance (m)
0
100
200
300
TWT (ns)
0
10
20
Depth (m)
B
440
460
480
500
Distance (m)
0
3.25
7.5
Depth (m)
0
50
100
150
TWT (ns)

Figure 9

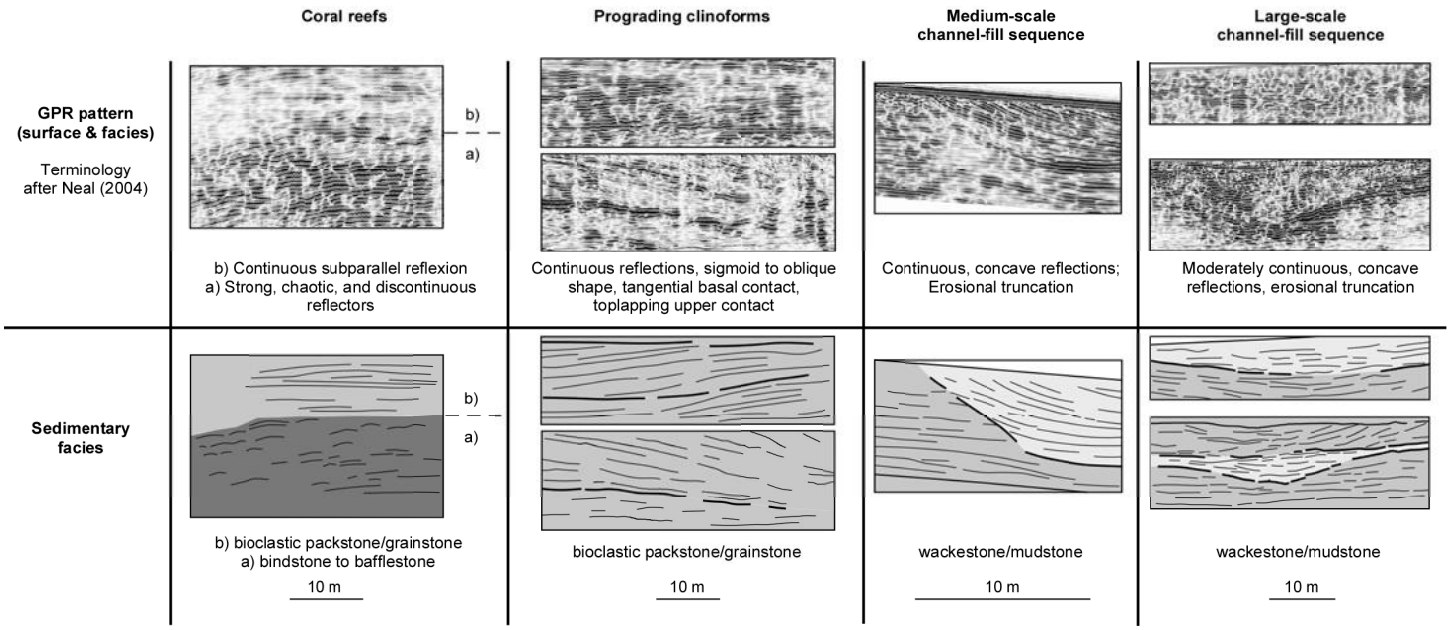
Coral reefs
Prograding clinoforms
Medium-scale channel-fill sequence
Large-scale channel-fill sequence
GPR pattern (surface & facies)
Terminology after Neal (2004)
b)
a)
b) Continuous subparallel reflexion
a) Strong, chaotic, and discontinuous reflectors
Continuous reflections, sigmoid to oblique shape, tangential basal contact, toplapping upper contact
Continuous, concave reflections; Erosional truncation
Moderately continuous, concave reflections, erosional truncation
Sedimentary facies
b)
a)
b) bioclastic packstone/grainstone
a) bindstone to bafflestone
bioclastic packstone/grainstone
wackestone/mudstone
wackestone/mudstone
10 m
10 m
10 m
10 m

Figure 10

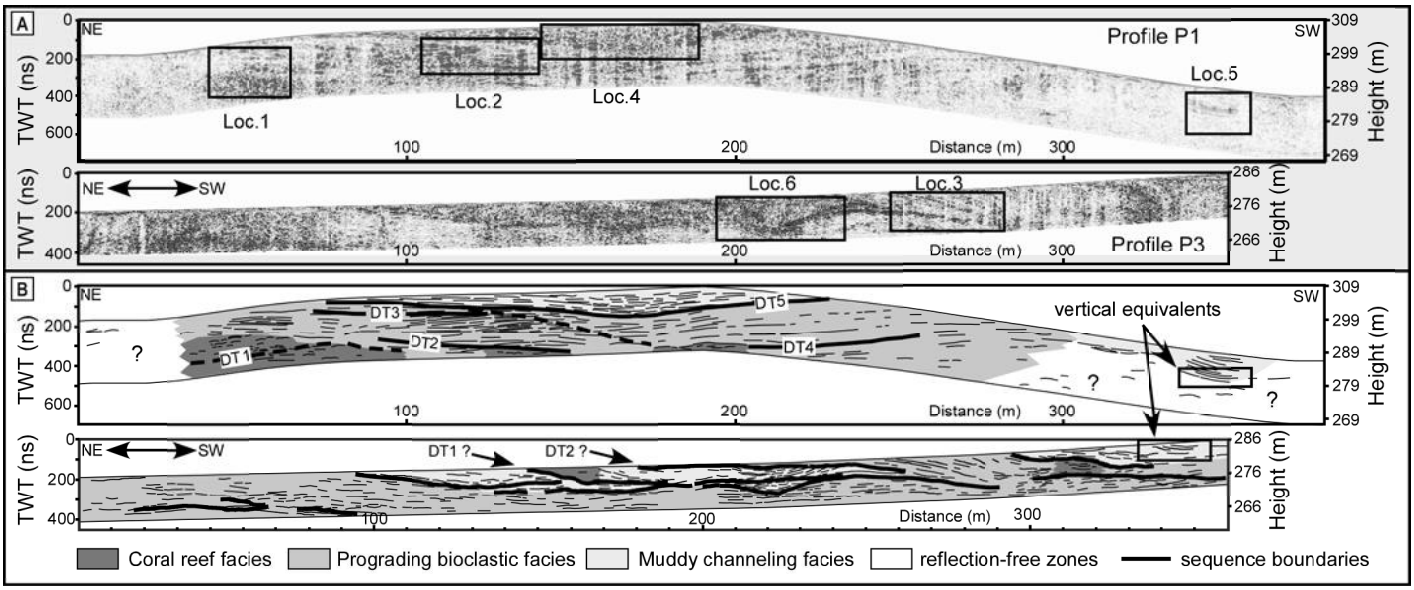
A
NE
SW
Profile P1
Loc.1
Loc.2
Loc.4
Loc.5
TWT (ns)
Height (m)
Distance (m)
NE
SW
Loc.6
Loc.3
Profile P3
B
DT1
DT2
DT3
DT4
DT5
vertical equivalents
DT1 ?
DT2 ?
Coral reef facies
Prograding bioclastic facies
Muddy channeling facies
reflection-free zones
sequence boundaries

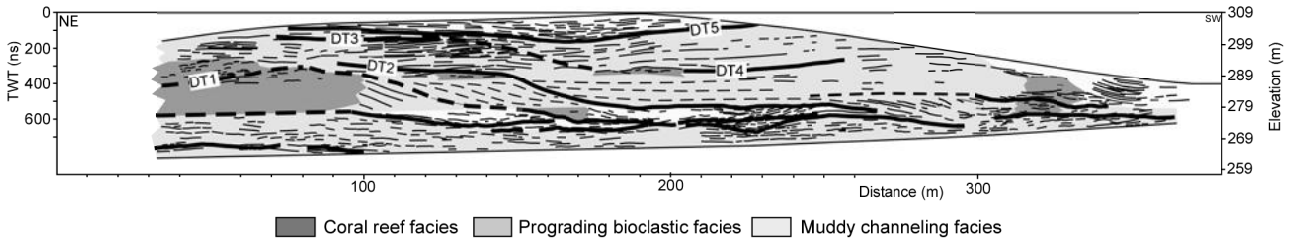
NE
SW
DT1
DT2
DT3
DT4
DT5
TWT (ns)
0
200
400
600
Elevation (m)
309
299
289
279
269
259
100
200
300
Distance (m)
Coral reef facies
Prograding bioclastic facies
Muddy channeling facies